

Hochschule für Angewandte Wissenschaften Hamburg
Fakultät Life Sciences

Expression, purification and biophysical characterization of SARS-CoV-2
non-structural protein 6.

Master Thesis
in pharmaceutical biotechnology

vorgelegt von
Jennifer Rothe



Hamburg
30.09.2022

Gutachter: Prof. Dr. Jörg Andrä (HAW Hamburg)

Gutachter: Prof. Dr. Jörg Labahn (Forschungszentrum Jülich)

Die Abschlussarbeit wurde betreut und erstellt im Labor des CSSB
in Zusammenarbeit mit dem Forschungszentrum Jülich

Abstract

The non-structural protein 6 (nsp6) is a membrane spanning protein and expressed by ORF1a of SARS-CoV-2. Nsp6 is likely to be involved in membrane anchoring of the replication complex but also to induce the formation of membrane structures to have impact on autophagy inhibition. It is predicted, that Nsp6 has a secondary structure consisting of alpha helices that span the lipid bilayer by 6 transmembrane domains and to have 3 luminal loops. Nsp6 has been shown to induce autophagosome formation from host ER and to have an inhibitory effect on lysosomal acidification through the interaction with ATP6AP1, causing autophagic flux stagnation to evade lysosomal degradation. Co-expression of Nsp3, Nsp4, and Nsp6 led to the formation of DMVs, in which Nsp6 mediate the association of DMVs with LDs and acts as a connector between the zippered ER and DMVs, in which it allows lipid flow but prevents access of ER proteins. In this work, Nsp6 was expressed into nanodiscs using a cell free expression system followed by purification using Ni-NTA affinity chromatography and size exclusion chromatography. The aim of this thesis was to characterize the primary, secondary and tertiary structure of Nsp6 using different biophysical methods. *In vitro* expression and purification of Nsp6 using nanodiscs of different sizes was successful allowing the characterization of primary, secondary and tertiary structure. It could be shown, that Nsp6 has a molecular size of around 34 kDa using MALDI-TOF mass spectrometry. Besides, mass photometry analysis revealed empty nanodiscs to have a higher molecular weight than Nsp6-MSP1E3D1-POPC complexes. Secondary structure analysis via CD spectroscopy confirmed the expected alpha helical structure. Deconvolution after subtraction of nanodisc from Nsp6-MSP2N2-POPC complex signal showed 75 % helical structure, whereas the alpha-fold model predicts 74 % helical and 4 % beta-structure. Tertiary structure analysis using fluorescence spectroscopy for tryptophan excitation revealed an emission maximum at 335 nm as expected for buried tryptophane residue in a properly folded protein. A higher fluorescence intensity of tyrosine and tryptophan compared to tryptophan fluorescence intensity, proved that not all tyrosine fluorescence is quenched by tryptophan, which indicates a high average distance between tryptophan and tyrosine in the protein structure.

Zusammenfassung

Das non-structural Protein 6 (Nsp6) ist ein membranspannendes Protein, welches vom ORF1a des SARS-CoV-2 exprimiert wird. Es ist wahrscheinlich, dass Nsp6 an der Membranverankerung des Replikationskomplexes beteiligt ist, aber auch die Bildung von Membranstrukturen induziert, die einen Einfluss auf die Autophagiehemmung haben. Es wurde vorhergesagt, dass Nsp6 eine Sekundärstruktur von Alpha-Helices hat, die die Lipiddoppelschicht durch sieben Transmembrandomänen durchspannen und 3 luminale Schleifen besitzen. Es wurde gezeigt, dass Nsp6 die Bildung von Autophagosomen aus dem ER des Wirts induziert und durch die Wechselwirkung mit ATP6AP1 eine hemmende Wirkung auf die lysosomale Ansäuerung hat, wodurch eine Stagnation des autophagischen Flusses verursacht wird, um dem lysosomalen Abbau zu entgehen. Die Koexpression von Nsp3, Nsp4 und Nsp6 führte zur Bildung von DMVs, in denen Nsp6 die Assoziation von DMVs mit LDs vermittelt und als Bindeglied zwischen dem Reißverschluss-ER und den DMVs fungiert, in denen es den Lipidfluss ermöglicht, aber den Zugang von ER-Proteinen verhindert. In dieser Arbeit wurde Nsp6 unter Verwendung eines zellfreien Expressionssystems in Nanodiscs exprimiert, gefolgt von einer Aufreinigung unter Verwendung von Ni-NTA Affinitätschromatographie und Größenausschlusschromatographie. Das Ziel dieser Arbeit war die Charakterisierung der Primär-, Sekundär- und Tertiärstruktur von Nsp6 durch Verwendung verschiedener biophysikalischer Methoden. Die In-vitro Expression und Aufreinigung von Nsp6 unter Verwendung von Nanodiscs unterschiedlicher Größe war erfolgreich und die Charakterisierung der Primär-, Sekundär- und Tertiärstrukturanalyse wurde durchgeführt. Mittels MALDI-TOF Massenspektrometrie konnte gezeigt werden, dass Nsp6 eine Molekülgröße von etwa 34 kDa hat. Außerdem ergab die massenphotometrische Analyse, dass leere Nanodiscs ein höheres Molekulargewicht als Nsp6-MSP1E3D1-POPC Komplexe aufweisen. Eine Sekundärstrukturanalyse mittels CD-Spektroskopie bestätigte die erwartete alpha-helikale Struktur des Nsp6. Dekonvolution nach Subtraktion des Nanodisc Signals vom Signal des Nsp6-MSP2N2-POPC Komplexes zeigte 75 % helikale Struktur, während das AlphaFold Modell 74 % helikale und 4 % beta-Struktur vorhersagt. Eine Tertiärstrukturanalyse unter Verwendung von Fluoreszenzspektroskopie zur Tryptophananregung ergab ein Emissionsmaximum bei 335 nm, wie es für einen verdeckten Tryptophanrest erwartet wurde. Eine höhere Fluoreszenzintensität von Tyrosin und Tryptophan im Vergleich zur Tryptophan

Fluoreszenzintensität bewies, dass nicht die gesamte Tyrosin-Fluoreszenz durch Tryptophan gelöscht wird, was auf einen hohen durchschnittlichen Abstand zwischen Tryptophan und Tyrosin in der Proteinstruktur hinweist.

Table of contents

I.	Abbreviations	1
II.	List of tables.....	2
III.	Table of figures.....	2
1	Introduction.....	3
1.1	Severe acute respiratory syndrome corona virus 2 (SARS-CoV-2)	3
1.1.1	Classification and pathogenesis	3
1.1.2	Virion and genome structure.....	4
1.1.3	Infectious life cycle.....	6
1.1.4	Non-structural proteins	8
2	Aim of Thesis	10
3	Material.....	11
3.1	Cells	11
3.1.1	Bacterial strains.....	11
3.2	Nucleic acids.....	11
3.2.1	Recombinant plasmids.....	11
3.3	Antibodies	11
3.3.1	Primary antibodies	11
3.4	Chemicals and reagents	11
3.5	Enzymes and associated buffer	12
3.6	Consumable supplies.....	13
3.7	Equipment.....	13
3.8	Standards and marker	13
3.9	Software and database	14
4	Methods.....	15
4.1	Nanodisc assembly.....	15
4.2	Protein production	15
4.2.1	In vivo protein production	15
4.2.2	In vitro protein production of Nsp6	16
4.3	DNA techniques.....	16
4.3.1	Preparation of plasmid DNA	16
4.3.2	Agarose gel-electrophoresis.....	17
4.3.3	Sanger sequencing	18
4.3.4	Transformation	18
4.4	Protein techniques.....	18
4.4.1	Affinity Chromatography	18
4.4.2	Size exclusion chromatography	22
4.4.3	PD10 buffer exchange	23
4.4.4	TEV-cleavage	23
4.4.5	SDS-PAGE	23
4.4.6	Western Blot analysis	24
4.5	Biophysical Methods	25
4.5.1	Circular dichroism and Fluorescence spectroscopy.....	25
4.5.2	Differential scanning fluorimetry	26
4.5.3	Mass photometry	27
4.5.4	Mass spectrometry	27
5	Results	28
5.1	Preparation of relevant proteins.....	28
5.1.1	Generation (expression and purification) of TEV protease	28
5.1.2	Generation of MSPs.....	29

Table of content

5.1.3	Nanodisc assembly with different MSPs	31
5.2	Generation of Nsp6-Nanodisc-complexes.....	33
5.3	Biophysical characterization of Nsp6 and Nsp6-Nanodisc-complexes	37
5.3.1	Analysis of the primary structure of Nsp6 and Nsp6-MSP1E3D1-POPC complexes	37
5.3.2	Analysis of secondary structure of Nsp6-nanodisc complexes via circular dichroism	40
5.3.3	Analysis of tertiary structure of Nsp6 and Nsp6-nanodisc complexes via fluorescence spectroscopy	43
6	Discussion.....	44
	Literature.....	48
	Eidesstattliche Erklärung	54

I. Abbreviations

ACE-2	Angiotensin-converting enzyme-2
DMV	Double membrane vesicle
gRNA	Viral genome
LB	Lysogeny broth
MWCO	Molecular weight cutoff
Nsp	Non-structural protein
ORF	Open reading frame
PAGE	Polyacrylamide gel electrophoresis
PMSF	Phenylmethylsulfonyl fluoride
RNP	Ribonucleoprotein
RO	Replication organelle
rpm	Rounds per minute
RTC	replication and transcription complex
SDS	Sodium dodecyl sulfate
S-protein	Spike protein
TBE buffer	Tris-borate-EDTA buffer
TEMED	Tetramethylethylenediamine
TMPRSS2	Transmembrane protease serine subtype 2
UTR	Untranslated region
v/v	Volume/volume
vRNA	Viral RNA
w/w	Weight/weight

II. List of tables

Table 1: Estimated secondary structure content.....	42
---	----

III. Table of figures

Figure 1: Classification and Taxonomy of <i>Coronaviridae</i>	3
Figure 2: Schematic structure of SARS-CoV-2.....	5
Figure 3: Genome structure of SARS-CoV-2.	6
Figure 4: Replication cycle of SARS-CoV-2.	7
Figure 5: Coomassie stain of TEV protease purification steps.	28
Figure 6: Coomassie stain of TEV protease activity test.	29
Figure 7: Analysis of MSP1E3D1 purification steps and TEV cleavage by Coomassie stain and Western Blot.....	30
Figure 8: Coomassie stain of MSP2N2 purification steps.....	31
Figure 9: Analysis of different assembled nanodiscs.	33
Figure 10: Western Blot analysis and SDS-PAGE of Nsp6-MSP1E3D1-POPC-complexes purification steps.....	35
Figure 11: Analysis of different Nsp6-nanodisc-complexes via SEC and SDS-PAGE.	36
Figure 12: Circular dichroism and fluorescence spectroscopy analysis of Nsp6-MSP1E3D1-POPC complexes.	40

1 Introduction

Human coronaviruses (HCoV) have appeared periodically around the world. The first coronavirus outbreak was severe acute respiratory syndrome coronavirus (SARS-CoV) in November 2002 in southern China [1]. It turned into a global infection in 2003 with a lethal rate of 9.6 % worldwide [2]. In the following decade, a second HCoV pandemic, caused by middle east respiratory syndrome coronavirus (MERS-CoV) occurred in June 2012 in Saudi Arabia [3]. In comparison to the first CoV outbreak, MERS showed a global fatality rate of 32.7 % [4]. Recently, a still ongoing third major HCoV outbreak occurred in December 2019 in the Wuhan province of China. The virus was classified as severe acute respiratory syndrome coronavirus 2 (SARS-CoV-2) leading to the new disease named coronavirus disease 2019 (COVID-19) [5]. In March 2020 the WHO officially declared the COVID-19 outbreak a pandemic [6]. To this day, over 600 million cases were reported of which 6.5 million were lethal (September 2022).

1.1 Severe acute respiratory syndrome corona virus 2 (SARS-CoV-2)

1.1.1 Classification and pathogenesis

Coronaviruses are large viruses that has a distinctive "crown-like" shape appearance. Current coronaviruses comprise 46 species in 26 subgenera and two subfamilies belonging to the family *Coronaviridae* [7]. SARS-CoV-2 belongs to the genus

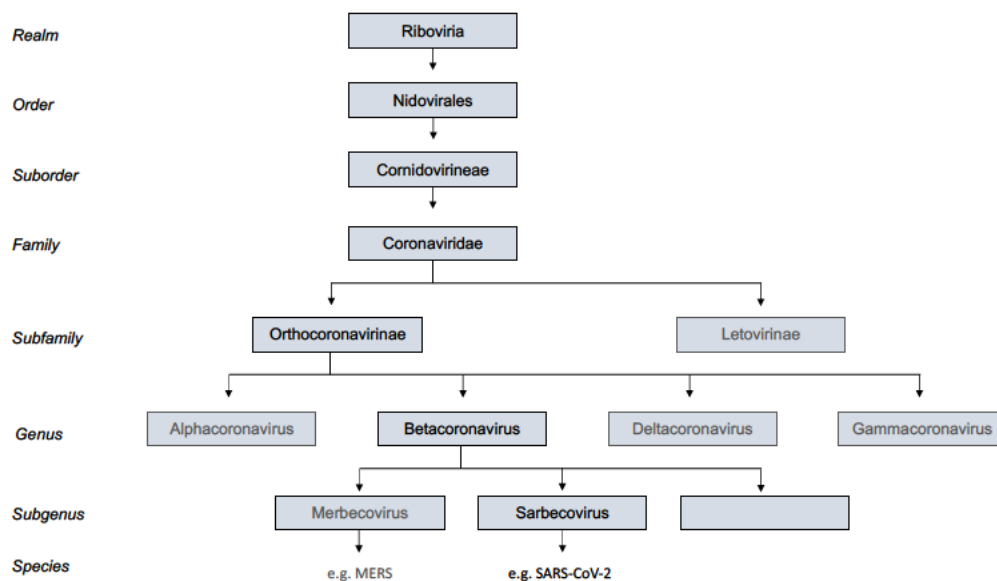


Figure 1: Classification and Taxonomy of Coronaviridae. This schematic representation displays a detailed phylogenetic tree of human coronaviruses, which were classified according to the International Committee of the Taxonomy of Viruses (ICTV) and the Coronaviridae Study Group (CSG) [7].

Betacoronavirus subgenus *Sarbecovirus* (Fig.1). The classification and taxonomy of the family *Coronaviridae* was developed by the *Coronaviridae* Study Group (CSG) of the ICTV [7].

Coronavirus infections can range from mild to severe or fatal outcome and can affect a variety of organs and systems. Typical symptoms include coughing, shortness of breathing, fever, loss of smell or taste and other flu-like symptoms [8]. The symptoms have been reported to appear after an incubation period of about 5.2 days [9]. A chest CT scan of patients reveals pneumonia, with abnormal features such as RNAemia (remaining viral RNA in blood), acute respiratory distress syndrome (ARDS) and acute cardiac injury [10][11]. In many cases a severe course of the disease caused ARDS and required ICU admission and oxygen therapy. In other cases it led to acute lung injury, damage to other organ systems and death [10][12]. Time from symptom onset of Covid-19 until death ranged from 6 to 41 days. However, incubation period among patients older than 70 years seemed to be longer than with younger patients [13]. Some people suffer from the so-called "long Covid", which results in persistent effects of infection or usual symptoms, even though patients have recovered from Covid-19. In addition, two-fifths of patients report a worsened quality of life [14].

1.1.2 Virion and genome structure

Coronaviruses are enveloped viruses with a positive single-stranded RNA genome and a roughly spherical or ellipsoidal shape with a diameter of 80-120 nm. Their particles comprise four structural proteins: spike (S), envelope (E), membrane (M), and nucleocapsid (N) (Fig. 2)[15]. The external lipid membrane of the virion is covered with spike proteins, which appears as a flexible head on a stalk with the ability to tilt up to 90 ° relative to the membrane [16]. The surface of the S trimer is heavily glycosylated, each of which S monomer contain 22 glycosylated sites. This glycan coat and the S trimers flexibility, enables SARS-CoV-2 to scan the host cell surface to bind the human host cell receptor angiotensin - converting enzyme-2 (ACE-2), while shielding the virus from neutralizing antibodies [17][18]. The binding of the S protein to its host cell receptor enables subsequent viral uptake and fusion. The viral outer membrane also contains the membrane protein (M) and envelope protein (E). Within the virion, ribonucleoprotein (RNP) complexes composed of the nucleocapsid protein (N) and the

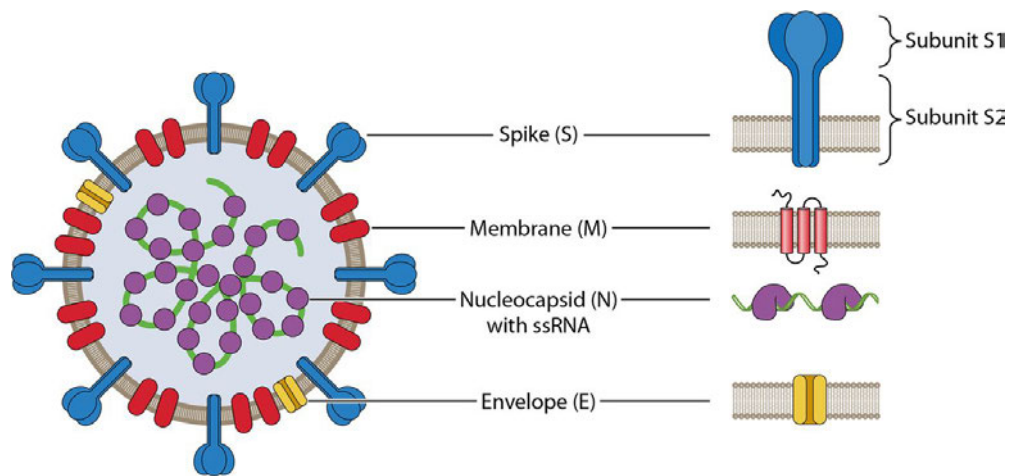


Figure 2: Schematic structure of SARS-CoV-2. Representation of the spherical shaped SARS-CoV-2 virion structure including the capsid proteins and the core proteins [41]

viral genome are present [19]. The E protein is a channel protein and part of the endoplasmic reticulum-Golgi intermediate compartment (ERGIC) membrane. In SARS-CoV-2 infection it mediates the budding and release of new virions [20].

Coronaviruses have the largest viral RNA genome amongst RNA viruses with a length of about 26 to 32 kb. The 30 kb SARS-CoV-2 genome shows a sequence identity of about 82 % with SARS-CoV and MERS-CoV and about 90 % sequence identity for essential enzymes and structural proteins. The RNA genome of the SARS-CoV-2 virus is composed of 13-15 open reading frames (ORFs) of which 12 are functional, flanked by two untranslated regions (UTRs) at the 5' and 3' end [21] (Fig. 3). The 5' ORF1a-1b translates two polyproteins pp1a and pp1ab and encodes for replicase, protease and 16 non-structural proteins (Nsp) being involved in the transcription and replication of SARS-CoV-2 [21][22]. ORF3a encodes proteins that induce necrotic cell death, while ORF6 expressed proteins limit interferon production and ORF7a encodes proteins crucial for the activation of nuclear factor- κ B (NF- κ B). The ORF8a and ORF9b expressed proteins trigger cellular apoptosis, whereas ORF8b proteins induces DNA synthesis and suppress viral envelope protein expression. ORF9b encodes proteins that alter interferon responses by manipulating host cell mitochondria and mitochondrial function to help evade host innate immunity [23]. The remaining ORFs encode for structural proteins known as spike (S), membrane (M), envelope (E), nucleocapsid (N) and hemagglutinin-esterase (HE) proteins [24][25]. The M, N and E proteins are required for virus morphogenesis, assembly and budding. Whereas the S-protein plays a vital role in the recognition of ACE-2 and mediates subsequent fusion of viral and host cellular membranes [26][27].

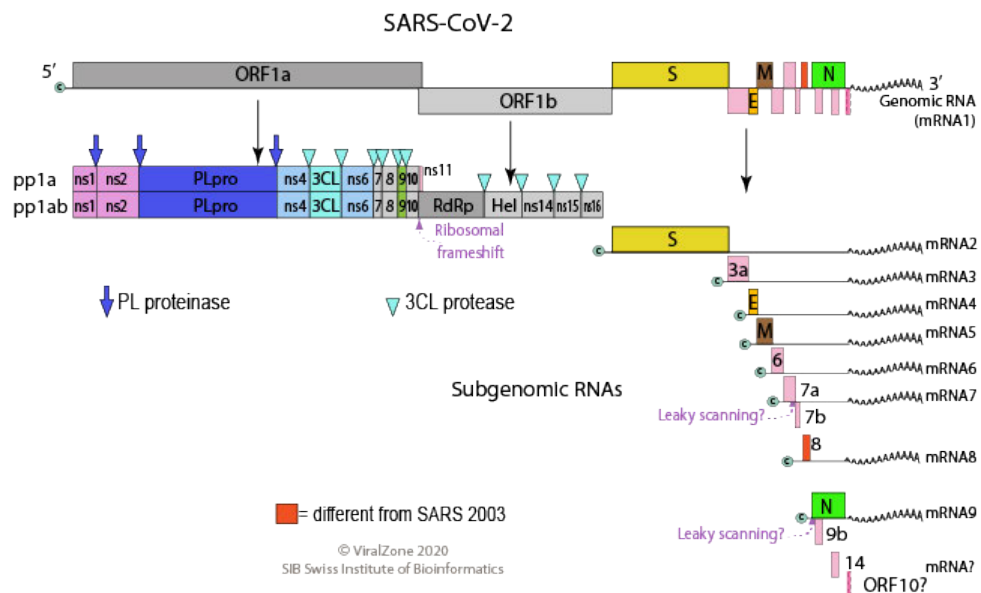


Figure 3: Genome structure of SARS-CoV-2. Schematic representation of the genome of SARS-CoV-2 demonstrating the different transcription units of the primary transcripts (ORF1a and ORF1b) and the subgenomic RNA unit created through discontinuous transcription.

The S-protein is made up of two subunits, the N-terminal domain S1 and the C-terminal domain S2. The S1 subunit comprises two subdomains, a N-terminal domain (NTD) and a C-terminal domain (CTD), which are able to function as receptor binding domains (RBDs), binding various proteins and sugars [28]. Besides, the S1 subunit consists of a distinct RBD and within it, a distinct receptor-binding motif (RBM), which is responsible for the initial docking to ACE-2 [29]. In contrast, the S2 subunit is responsible for viral fusion and entry via fusion peptide, heptapeptide repeat sequence 1 (HR1), HR2, transmembrane domain and cytoplasm domain [30]. Among all alpha- and betacoronaviruses, the Spike protein is cleaved by furin (a host protease) between the S1 and S2 domain [28].

1.1.3 Infectious life cycle

The uptake of SARS-CoV-2 into the host cell is initiated by its host cell surface receptor ACE-2, which is expressed on epithelial cells of the lung and intestines, and to a lesser extent, in the heart, kidney, adipose, and both male and female reproductive tissues. The binding to ACE-2 is facilitated by the spike protein of SARS-CoV-2. As soon as the SARS-CoV-2 spike protein is about to bind to the ACE-2 receptor protein, it needs to get proteolytically activated at the S1/S2 sites [31]. The spike proteins of SARS-CoV and MERS-CoV are activated through the cleavage by host transmembrane serine

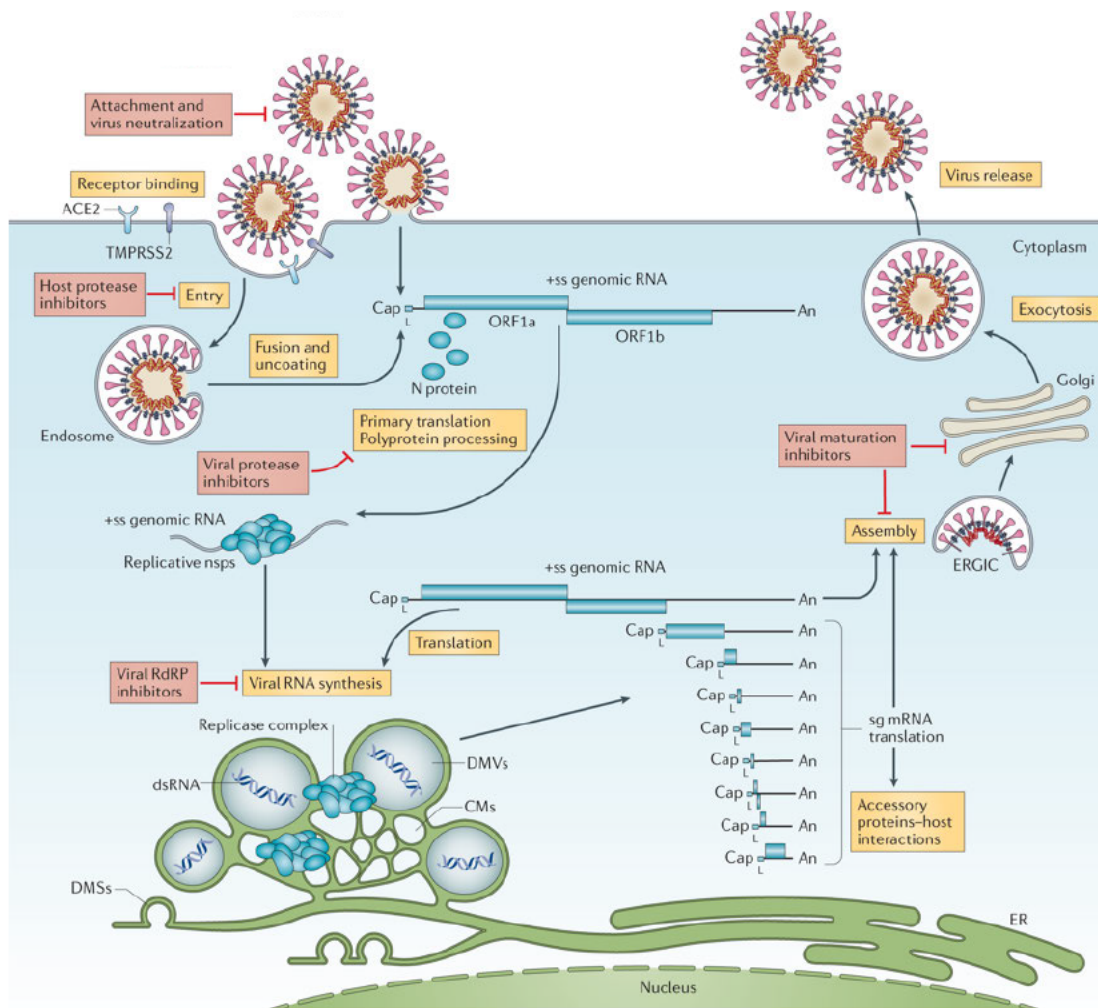


Figure 4: Replication cycle of SARS-CoV-2. The SARS-CoV-2 spike protein binds to ACE-2, which activates proteases to activate its S1/S2 subunits. Activation of spike subunits triggers conformational changes, leading to viral fusion with the host cell. After uncoating, the viral genome is transferred to the nucleus, where DNA replication takes place. In the absence of aforementioned proteases, viral uptake is triggered by cathepsin L-mediated endocytosis. After fusion with the membrane, viral genome is released into the cytoplasm. Viral genome is capped and ORF1a/b are translated immediately, followed by non-structural proteins. Viral RNA synthesis takes place in replication organelles formed in the host cytoplasm formed of ER-derived double-membrane vesicles in cooperation with Nsp3, Nsp4 and Nsp6. After structural proteins are translated, they interact with newly produced RNA leading to budding into the lumen of secretory vesicular compartments. [37]

protease TMPRSS2. Providing a preliminary priming step for the viral entry, the activation of SARS-CoV-2 spike protein relies on TMPRSS2 protease [32][33]. Besides, it is speculated that a pre-cleavage at the S1/S2 sites, mediated by the cellular cysteine protease furin might promote subsequent TMPRSS2-dependent cell entry [34]. After cleavage, the spike protein binds to the ACE-2 receptor and a protease cleavage at the S2' site of the spike protein occurs, leading to the exposure of the viral fusion protein FP1-2. Subsequently, ionic changes promote conformational changes and fusion peptide insertion, driving the fusion of SARS-CoV-2 membrane with the

host cell membrane (early pathway). The viral genome is transferred into the host cell cytoplasm where the viral replication takes place (Fig. 4) [35]. In the absence of the beforementioned proteases, the virus entry is built on the endocytosis pathway (late pathway), where the fusogenic activation of the spike protein occur through cathepsin L (CTSL) of the lysosome. The low-pH environment in the endosome activates CTSL and triggers the fusion of the viral membrane with the endosome membrane, leading to the release of the viral genome into the cytoplasm [36].

After the viral genome (gRNA) uptake into the cell, gRNA is capped on its 5' end and polyadenylated on its 3' end. ORF1a and ORF1b, are immediately translated in polyproteins pp1a and pp1ab. Nsp3 and Nsp5 cleave pp1a and pp1ab into 16 non-structural proteins which form the viral replication and transcription complex (RTC) [37]. The synthesis of the viral RNA (vRNA) takes place in the cytoplasm of the host cell utilizing intracellular membranes, forming replication organelles (ROs). Such membranous structures may take the shape of ER-derived atypical structured double-membrane vesicles (DMVs), convoluted membranes (CMs) and the recently discovered double-membrane spherules (DMSs) [38][39]. The membrane-spanning Nsp3, Nsp4, and Nsp6 have been proven to be involved into the construction of these replication organelles. These subcellular structures provide optimal platforms for vRNA synthesis, harboring viral replicative proteins and relevant host factors. Besides, ROs can hide replication intermediates, helping to create smaller canonical autophagosomes and consequently to evade the innate immune sensors that can detect dsRNA [40]. After the viral structural proteins are translated, they relocate into the endoplasmic reticulum (ER) membranes to transit the ER-to-Golgi intermediate compartment (ERGIC). Following, they interact with N-encapsidated, newly produced genomic RNA, leading to budding into the lumen of secretory vesicular compartments [38]. Finally, new virions are assembled and secreted out of the infected cell via exocytosis.

1.1.4 Non-structural proteins

1.1.4.1 Nsp3 and Nsp4

Nsp3 and Nsp4 are membrane spanning proteins expressed by the ORF1a of SARS-CoV-2. Nsp3 is released from pp1a/1ab by the papain-like protease domain(s), which is part of Nsp3 itself. Nsp3 including papain-like proteinase activity to act with itself, deubiquitinating activity, and ADP-ribose-1"-phosphatase activity [41]. Nsp3

releases Nsp1, Nsp2, and itself from pp1a/1ab and interacts with other viral Nsp's as well as RNA to form the replication and transcription complex (RTC). The RTC formation is associated with modified host ER membranes that produce convoluted membranes (CMs) and double-membrane vesicles (DMVs) in SARS-CoV-2 [38][39]. Nsp4 is a transmembrane glycoprotein and is known to play a role in formation of the double-membrane vesicles associated with replication complexes. Co-transfection of Nsp3 with Nsp4 indicates an effect on membrane conformation, leading to a walled, maze-liked, perinuclear double-membrane structure [42].

1.1.4.2 Nsp6

Additionally, a third integral membrane non-structural protein (nsp6) is expressed by ORF1a of SARS-CoV-2. It has been suggested to span the membrane several times and is likely to be involved in membrane anchoring of the replication complex but also to induce the formation of membrane structures and inhibition of autophagy. It is predicted by a model, that Nsp6 spans the lipid bilayer by seven transmembrane domains and to have 3 luminal loops [42]. Besides, it is predicted to contain N-glycosylation sites between the fifth and sixth hydrophobic domains. Like Nsp3 and Nsp4, Nsp6 does not contain N-terminal signal sequences for co-translational membrane insertion [43]. Nsp6 has been shown to induce autophagosome formation from host endoplasmic reticulum and to have an inhibitory effect on lysosomal acidification through the interaction with ATP6AP1. Through the inhibition of ATP6AP1 cleavage-mediated activation, an autophagic flux stagnation to evade lysosomal degradation is caused [44][45]. Besides, SARS-CoV-2 infected Hela-cells showed smaller autophagosomes than starved cells. Recent studies showed that the co-expression of Nsp3, Nsp4, and Nsp6 led to the formation of DMVs. It was found that Nsp6 zippers the ER and mediates the association of DMVs with LDs. Nsp6 also is likely to work as a connector between the zippered ER and DMVs, in which it allows lipid flow but preventing access of ER proteins [46]. But as mentioned before, the co-expression of Nsp3 and Nsp4 alone contained so-called maze-like bodies (MLBs). Therefore, it was concluded that Nsp6 is essential for the generation of SARS-CoV-2 DMVs, whereas Nsp3 and Nsp4 just mediate the pairing of membranes for DMV formation [41]. HEK293T transfection with Nsp6 alone induces small spherical vesicles with single membranes that cluster around the microtubule organizing center [41].

2 Aim of Thesis

Since the start of the COVID-19 pandemic, research has been strongly focused on obtaining a complete understanding of the biology of the viral infection, in order to develop vaccines and therapeutic approaches. In particular, structural studies of the SARS-CoV-2 proteins have helped to make progress towards treatment and preventative therapeutics against COVID-19. However, many knowledge gaps on the structural biology and function of some SARS-CoV-2 proteins still remain such as for non-structural protein 6. Hence, in this work the expression of Nsp6 into nanodiscs using cell free expression system and the purification of Nsp6 in nanodiscs via a two-step purification using affinity chromatography and size exclusion chromatography should be performed. Purified Nsp6-nanodiscs complexes should be used to characterize the primary, secondary and tertiary structure of Nsp6 using different biophysical methods. This study should help to provide a base for future studies on SARS-CoV-2 treatment by interference of viral replication.

3 Material

3.1 Cells

3.1.1 Bacterial strains

Strain	characteristics
Top10	F - mcrA Δ (mrr-hsdRMS-mcrBC) ϕ 80lacZ Δ M15 Δ lacX74 recA1 araD139 Δ (araleu)7697 galU galK rpsL (Str R) endA1 nupG
BL21(DE)	F - ompT hsdSB (rB - mB -) gal dcm (DE3)

3.2 Nucleic acids

3.2.1 Recombinant plasmids

The following plasmids were used for gene expression or protein expression *in vivo* and *in vitro*.

#	Name	Purpose	Reference
75	pET28a-N-7*his-MSP1E3D1	Protein expression in	Group database
76	pET28a-N-7*his-MSP2N2	Protein expression in BL21(DE)	Group database
	pET28a-N-7*his-Nsp6	Gene expression in Top10 and protein expression <i>in vitro</i>	Group database
54	pMal-C2-TEVprotease	Protein expression in BL21(DE)	Group database

3.3 Antibodies

3.3.1 Primary antibodies

Name	Properties	Reference
His-probe (H-15)	Polyclonal rabbit antibody against polyhistidine domains of pET	Santa Cruz, sc-803

3.4 Chemicals and reagents

Name	Company
Acrylamide 4K - Solution (30 %)	AppliChem
AEBSF hydrochloride	Th Geyer
Agarose	Roth

Material

Benzamidine hydrochloride	Sigma-Aldrich
Bromphenol blue	Sigma-Aldrich
Carbenicillin Dinatriumsalz	VWR
Coomassie® Brilliant blue G-250	Merck
DNase I	AppliChem
E-64	Roth
EDTA	AppliChem
Ethanol 99,9 % for HPLC	VWR
Ethanol 96 %	AppliChem
DTT	Roth
Fos-cholin-16	Anatrace
Glycerol	AppliChem
GelRed	VWR
HEPES	AppliChem
Imidazole PUFFERAN® ≥99 %	Roth
Isopropanol for analysis	Roth
Leupeptin	Roth
Lysozyme BioChemica	AppliChem
Non-fat dry milk powder	AppliChem
Pepstatin	Roth
PMSF	AppliChem
TEMED	AppliChem
Tris Base/ Tris HCl	AppliChem
Triton-X100	AppliChem
Trypan blue	Merck
Tween® 20	AppliChem

3.5 Enzymes and associated buffer

Name	Company
FastDigest Green Puffer [10x]	ThermoFischer Scientific
FastDigest EcoRI	ThermoFischer Scientific
FastDigest NdeI	ThermoFischer Scientific

3.6 Consumable supplies

Name	Company
Centrifugal filters Amicon	Merck
Micro cuvettes	Sarstedt
MEMBRANE AMERSHAM HYBOND 0,45µM PVDF	Th Geyer
Monolith NT.115 Premium Capillaries	Nanotemper
PCR tubes	VWR
Pipette tips (20 µl, 200 µl, 1000 µl)	Sarstedt
Polystyrene tubes (15 ml, 50 ml)	Sarstedt
Reaction tubes (1.5 ml, 2 ml)	Sarstedt
Whatman Paper	VWR

3.7 Equipment

Name	Company
Äkta Explorer	Pharmacia Biotech
Autoflex maX	Bruker
Aviv 420 Circular Dichroism Spectrometer	Biomedical Inc.
Centrifuge 5804R	Eppendorf
Centrifuge 5417R	Eppendorf
Centrifuge LYNX 6000	ThermoFischer Scientific
ChemiDoc MP Imaging System	BioRad
Innova 4200 Incubator	New Brunswick
Nanotemper Prometheus NT.48 fluorimeter	Nanotemper
Multitron incubator	Infors HT
NanoDrop 1000 spectrometer	ThermoFischer Scientific
Refeyn TwoMP mass photometer	Refeyn
Superose 6 increase 10/300 GL	Cytiva
Trans-Blot Turbo Transfer System	BioRad
Ultracentrifuge Optima XPN-90	Beckman Coulter

3.8 Standards and marker

Product	Company
1 kb and 100 bp DNA ladder	ThermoFischer Scientific
Prestained Protein Ladder	JenaBioscience

3.9 Software and database

Software	Purpose	Reference
<i>flexControl software</i>	MS Data acquisition	Bruker
<i>flexAnalysis software</i>	MS Data analysis	Bruker
ImageLab	Band intensity determination	BioRad
Mendeley Desktop 1.19.4.	Reference management	Mendeley Ltd
Origin 2020	CD/FL, DSF data analysis	OriginLab
PubMed	Literature database	Open software (provided by NCBI)
PhotoMol	Mass photometry data analysis	spc.embl-hamburg.de
Word	Text Processing	Microsoft Office

4 Methods

4.1 Nanodisc assembly

Nanodiscs are made up of two Membrane scaffold proteins (MSPs), that incorporate lipids to create an unnatural lipid bilayer. In this study the two different MSPs MSP1E3D1 and MSP2N2 were used to incorporate 1-palmitoyl-2-oleoyl-glycero-3-phosphocholine (POPC). Prior to the preparation of the Nanodiscs, lipids were solubilized in 100 mM sodium cholate buffer (in Milli-Q[®] water) to a concentration of 30 – 40 mg/mL. Afterwards, 250 μ L ND buffer, 250 μ L sodium cholate buffer and POPC lipids in a ratio of 1:130 or 1:240 (v/v) were added to 2 mg MSP1E3D1 or MSP2N2 (4 mg/ml in 500 mL), respectively. The reaction solution was incubated for 1.5 h at 4 °C while rotating. In order to get rid of the sodium cholate in the buffer, the reaction solution was transferred to a 12 - 14 K MWCO dialysis membrane and incubated in ND Buffer for about 35 h at 4 °C. The dialysis buffer was change to fresh 5 L ND buffer every 8 - 15 h. After the dialysis, samples were concentrated in 10 kDa centrifugal filters (Amicon[®], Merck) to around 450 μ L. The sample was filtrated in a 0.2 μ m centrifugal filter (Nanosep[®] MF, Pall) at 20.000 xg (Centrifuge 5417R, Eppendorf) and injected to a gelfiltration column (see 4.4.1.2.), pooled and concentrated in a 50 kDa centrifugal filter (Amicon[®], Merck) to 13 – 20 mg/mL.

4.2 Protein production

4.2.1 In vivo protein production

4.2.1.1 TEV protease

To prepare the pre-culture, some colonies were picked from agar and incubated in 60 mL LB medium with 2 % glucose, 34 μ g/ μ L chloramphenicol and 100 μ g/ μ L ampicillin for around 5 h at 37 °C 180 rpm (Innova 4200, New Brunswick). Afterwards, main culture was prepared with 500 mL LB medium, 100 μ g/ μ L ampicillin, 34 μ g/ μ L chloramphenicol and 5 mL of pre-culture. Main culture was incubated for 12 h at 37 °C and 120 rpm (Multitron, Infors HT). After 12 h and at an OD₆₀₀ of 0.5 the temperature was decreased to 30 °C. At an OD₆₀₀ of 7 the culture was induced with 1 mM IPTG and incubated for 6 h at 30 °C and 120 rpm (Multitron, Infors HT). Cells were harvested by centrifugation for 20 min at RT and 5000 xg (LYNX 6000, Thermofischer).

4.2.1.2 Membrane Scaffold proteins

To prepare the pre-culture, all colonies from MSP1E3D1 and MSP2N2 transformation were picked from agar and incubated in 50 mL TB media containing 10 % KPI buffer (0.72 M K₂HPO₄, 0.17 M KH₂PO₄) and 0.2 % glucose and 30 µg/µL kanamycin at 37 °C and 180 rpm (Innova 4200, New Brunswick) to an OD₆₀₀ of 4. For main culture, 300 mL TB with KPI, 0.2 % glucose, 30 µg/µL Kanamycin and 4 mL pre-culture were incubated at 37 °C and 110 rpm (Multitron, Infors HT). At OD₆₀₀ 0.5 the temperature was decreased to 26 °C and the culture was induced with 1 mM IPTG at an OD₆₀₀ of 1 and further grown for 3 h and 110 rpm. Cells were harvested by centrifugation for 20 min at RT and 4000 xg (LYNX 6000, Thermofischer) and stored at -80 °C.

4.2.2 In vitro protein production of Nsp6

In vitro translation was performed 40 times in a 25 µL reaction volume using HiYield-T7 E. coli lysate (CubeBiotech). The reaction was assembled using following consumables (see Table below).

Consumables	Volume (µL)
E. coli extract	8.75
Reaction Buffer	10
IPTG (50 mM stock)	0.5
EDTA-free Protease Inhibitor Tablet	0.5
Nanodisc	15 µg
Plasmid	0.5 µg
RNase free water	Make up to 25 µL

The reaction was incubated for 3 h at 30 °C and 600 rpm on a thermocycler. After the incubation the reaction mix was pelleted down for 30 min at 4 °C and 20.000 xg (Centrifuge 5417R, Eppendorf).

4.3 DNA techniques

4.3.1 Preparation of plasmid DNA

Plasmid DNA was isolated by using the *GeneJET Plasmid-Maxiprep-Kit* (Thermofischer). 300 mL LB medium (supplemented with 100 µg/mL carbenicillin) was inoculated with 30 µL pre-culture that was isolated from a single bacterial colony and incubated for 12 - 14 h at 37 °C (Multitron, Infors HT). Bacteria were sedimented for 20 min at 4 °C and 4000 xg (LYNX 6000, Thermofischer) and the pellet was transferred to 50 mL Falcon tubes (Sarstedt) and the supernatant was discarded. The bacterial

pellet was resuspended in 6 mL resuspension solution with RNase A (40 μ L per 1 mL resuspension solution). 6 mL lysis solution was added, the solution was inverted 4 - 6 times and incubated at room temperature for 3 min. Next, 6 mL neutralization solution was added and the solution was inverted 5-8 times until it turned colorless. Afterwards, 0.8 mL Endotoxin Binding Reagent was added and mixed 5 - 8 times. After an incubation for 5 min at RT 6 mL 96 % ethanol was added and mixed 5 - 6 times. The sample was centrifuged for 40 min at 4 °C and 4000 xg (Centrifuge 5804R, Eppendorf). The supernatant was then transferred to a new 50 mL falcon and 6 mL 96 % ethanol were added and mixed 5-6 times. The sample was applied to the column and centrifuged for 3 min at 4 °C and 2000 xg. The column was washed with wash solution 1 and centrifuged for 2 min at 4 °C and 3000 xg (Centrifuge 5804R, Eppendorf) in a swinging bucket rotor. The flow-through was discarded and the column was washed two times with wash solution 2, followed by centrifugation for 2 min at 4 °C and 3000 xg after each washing step. Plasmid DNA was eluted 2 - 3 times with 500 μ L elution buffer into a sterile 50 mL falcon tube. Eluted DNA was supplemented with 1/10 volumes ice cold sodium acetate and 2 volumes ice cold 99 % ethanol and stored ON at -80 °C. The next day, the solution was centrifuged for 30 min at 4 °C and 20.000 xg (Centrifuge 5417R, Eppendorf) to pellet down the plasmid DNA. The supernatant was discarded, the DNA pellet was washed with 300 μ L of 75 % ethanol and centrifuged at for 10 min at 4 °C and 20.000 xg followed by the same washing step but with 99 % ethanol. At last, the ethanol was discarded and the DNA pellet was air-dried and resuspended in 500 μ L double distilled H₂O (ddH₂O). To determine the DNA concentration, 2 μ L of eluted DNA was applied to the spectrometer NanoDrop 2000 (Thermofisher).

4.3.2 Agarose gel-electrophoresis

Analytical gels were prepared by dissolving agarose powder in 1x TBE buffer to a final concentration of 1 % using a microwave. After boiling, the agarose solution was supplemented with *Gelred*[®] (Thermofischer) and poured into an appropriate gel tray with a well comb in place. The solidified gel was placed into the electrophoresis device filled with 1x TBE. The DNA samples are pre-mixed with *FastDigest Green Buffer* (10x, Thermofischer) That allows for direct loading of reaction mixtures to the agarose gel. A 1 kb DNA ladder (Thermofischer) was applied as a size reference. Electrophoresis

was performed at 80 V. DNA fragments were visualized by applying UV light using the *ChemiDoc™ MP* (BioRad).

4.3.3 Sanger sequencing

For sequencing, 1 µg DNA was transferred to a 1.5 mL reaction tube. Sequencing was performed by Microsynth Seqlab (Göttingen).

4.3.4 Transformation

Prior to transformation 100 µL chemical competent *E. coli* BL21(DE) were unfrozen on ice and mixed with 1 - 2 µL plasmid and incubated on ice for 20 min. A heat shock at 42 °C for 2 min on a heat block (Thermofischer) was performed followed by an incubation step for 2 min on ice. Next, 900 µL LB medium without antibiotics was added to the bacterial suspension. After an incubation at 300 rpm and 37 °C for 45 min on a heat block (Thermofischer), the suspension was centrifuged at 15000 rpm for 1 min (Centrifuge 5417R, Eppendorf) and 900 µL supernatant was discarded. The pellet was resuspended in the remaining 100 µL LB media and plated on LB agar and incubated at 37 °C overnight.

4.4 Protein techniques

4.4.1 Affinity Chromatography

Affinity chromatography is a separation technique based on a specific macromolecular binding interaction between an immobilized ligand or substrate and its binding partner. The used proteins in this study all comprise an N-terminal his-tag, which leads them to interact with metal ions. His-tag purification uses the purification method of immobilized metal affinity chromatography (IMAC). In this work, Ni-NTA agarose resin (CubeBiotech) was used for IMAC. Ni-NTA refers to the transition metal ion nickel²⁺ that is immobilized on a resin matrix using the chelating agent nitrilotriacetic acid (NTA).

4.4.1.1 Purification TEV-protease

15 g Cell pellet was resuspended for 1 h at 4 °C in 200 ml Lysis buffer. Cells were opened using a cell disruptor (Avestin) with pressure between 15000 – 20000 psi followed by ultracentrifugation for 30 min at 4 °C and 50.000 xg (Centrifuge 5804R, Eppendorf). The Supernatant was filtered through 0.45 µm filter, added to

pre-equilibrated 10 ml indigo Ni-NTA resin and incubated for 2 h at 4 °C while stirring. After loading the resin-protein mixture to a column, the flow-through was collected using low flowrate. The resin was washed with 50 CV Lysis buffer and first eluted with 3 CV elution buffer 1. Next, a second elution was done using 6 CV elution buffer 2 and elution buffer 3. After elution, 1 mM EDTA and 1 mM DTT was immediately added to the eluted samples and concentrated with 3 kDa centrifugal filters (Amicon®, Merck) at 4000 xg to 2.67 mg/mL, aliquoted and stored at -80 °C. 100 µL sample of each step were collected for SDS-PAGE and western blot analysis.

Lysis buffer	20 mM Tris-HCl, pH 8 500 mM NaCl 10mM Imidazole 1mg/mL Lysozyme 5mg/50g Cell Pellet DNase I
Elution buffer 1	20 mM Tris-HCl, pH 8 0.5 M NaCl 10% Glycerin 100 mM Imidazol
Elution buffer 2	20 mM Tris-HCl, pH 8 0.5 M NaCl 10% Glycerin 300 mM Imidazol
Elution buffer 3	20 mM Tris-HCl, pH 8 0.5 M NaCl 10% Glycerin 750 mM Imidazol

4.4.1.2 Purification of MSPs

Cell pellet (10 g MSP2N2, 11 g MSP1E3D1) was unfrozen on ice and resuspended in 100 mL Lysis Buffer while stirring for 20 min at 4 °C. 10 mL of 50 % Ni-NTA resin (in 20 % ethanol) was added to a column, washed with MilliQ and equilibrated with Lysis buffer. Cells were opened using the cell disruptor at 15000 – 20000 bar followed by ultracentrifugation for 30 min at 4 °C and 30.000 xg (Optima XPN-90, Beckman Coulter). The supernatant was loaded to the column and incubated for 3.5 h at 4 °C while shaking. The flowthrough was collected using a low flowrate. The column was washed with wash buffer 1 using low flowrate, followed by wash buffer 2 using increasing flowrate during wash and finally with wash buffer 3 using high flowrate.

MSPs were eluted by adding 2 CV elution buffer and incubation for about 10 min. Elution was done using low flowrate. Subsequently, another 2 CV elution buffer were added and immediately eluted. Elution was repeated using in total 6 CV are used up. The elution fraction steps were combined and concentrated to 5 mL using 10 kDa centrifugal filters (Amicon®, Merck) at 3900 xg. 50 µL sample of each step was collected for SDS-PAGE and western blot analysis.

After concentrating the MSPs, buffer was exchanged to TEV-cleavage buffer using a Sephadex g25 PD10 desalting column (Cytiva)(see 4.4.3.) which was followed by TEV-cleavage of MSPs (see 4.4.4.). Cleaved MSPs were applied to a 5 mL Ni-NTA column equilibrated with TEV-cleavage buffer. Flow-through containing cleaved MSPs was collected. The column was washed with 5 CV MSP storage buffer (supplemented with 10 mM imidazole). The wash was collected together with the flow-through. Flow-through was concentrated in 10 kDa centrifugal filters (Amicon®, Merck) to 5 mL and again applied to a Sephadex g25 PD10 desalting column to exchange to MSP storage buffer. MSP concentration was determined via NanoDrop 2000 (Thermofischer) and concentrated to around 4 mg/mL. Finally, 500 µL of 4 mg/mL MSP were stored at -80 °C until application for Nanodisc assembly (see 4.1.).

Lysis Buffer	40 mM Tris-HCl, pH 8 300 mM NaCl 1 % Triton X-100 1 µg/µL DNase 1 1 mg/mL Lysozyme Protease Inhibitors
Wash Buffer 1 (10 CV)	40 mM Tris-HCl, pH 8 300 mM NaCl 1 % Triton X-100
Wash Buffer 2 (10 CV)	40 mM Tris-HCl, pH 8 300 mM NaCl 20 mM Imidazole 50 mM Sodium cholate
Wash Buffer 3 (10 CV)	40 mM Tris-HCl, pH 8 300 mM NaCl 50 mM Imidazole
Elution Buffer (6 CV)	40 mM Tris-HCl, pH 8 300 mM NaCl 500 mM Imidazole

4.4.1.3 Purification Nsp6

After in vitro expression, samples were pelleted for 30 min at 4 °C and 20.000 xg (Centrifuge 5417R, Eppendorf). 1 mL supernatant mixed with 8 mL equilibration buffer was added to 3 ml of pre-equilibrated 50 % Ni-NTA resin and incubated over night at 4 °C while shaking. The flow through was collected and reapplied to the column 6 times. The resin was washed with 13 CV of wash buffer 1, wash buffer 2 and wash buffer 3, respectively. Subsequently, the column was washed 2 times with 6.5 CV of wash buffer 4 and wash buffer 5. Finally, 1 CV elution buffer was added to the resin and incubated for 10 min and the Nsp6-nanodisc complexes were eluted with the flow-through. Another 1 CV elution buffer was added immediately and eluted. Elution step was repeated until 8 CV elution buffer were used up. 60 µL of each purification step were collected for SDS-PAGE and western blot analysis.

Equilibration Buffer / Wash buffer 1	20 mM HEPES, pH 7.8 150 mM NaCl 10 % Glycerol 1 mM TCEP 15 mM Imidazole Protease Inhibitors
Wash buffer 2	20 mM HEPES, pH 7.8 150 mM NaCl 10 % Glycerol 1 mM TCEP 20 mM Imidazole Protease Inhibitors
Wash buffer 3	20 mM HEPES, pH 7.8 500 mM NaCl 10 % Glycerol 1 mM TCEP 20 mM Imidazole Protease Inhibitors
Wash buffer 4	20 mM HEPES, pH 7.8 1000 mM NaCl 10 % Glycerol 1 mM TCEP 20 mM Imidazole Protease Inhibitors
Wash buffer 5	20 mM HEPES, pH 7.8 150 mM NaCl

10 % Glycerol
1 mM TCEP
25 mM Imidazole
Protease Inhibitors

Elution buffer

20 mM HEPES, pH 7.8
150 mM NaCl
10 % Glycerol
1 mM TCEP
500 mM Imidazole
Protease Inhibitors

Protease Inhibitors	Final concentration
AEBSF	1 mM
Benzamidine	1 mM
E-64	1 mM
Leupeptin	1 mM
Pepstatin A	1 mM
PMSF	0.2 mM

4.4.2 Size exclusion chromatography

During size exclusion chromatography (SEC), molecules in solution can be separated according to their size. The column is packed with a gel filtration matrix with a definite pore size distribution. The molecules go through the column in different paths according to their sizes, which leads larger molecules (whose size is larger than the biggest pore) going through the interspaces of the gels. In contrast, smaller molecules run through the interior of the gel pores, leading to greater retention time. The smaller the molecular size, the more pores the molecule can pass through. That implies, that the largest molecules pass through the column first, while the smaller ones come last, leading to a size separation. In this work, a Superose 6 increase 10/300 GL (Cytiva) column was used to separate desired proteins. First of all, eluted Nsp6-Nanodisc complexes were concentrated in 50 kDa centrifugal filters (Amicon[®], Merck) to 450 μ L at 3900 xg (Centrifuge 58904R, Eppendorf). Immediately, sample was filtered in a 0.2 μ m centrifugal filter (Nanosep[®] MF, Pall) at 20.000 xg (Centrifuge 5417R, Eppendorf) and injected to a 500 μ L sample loop to the Äkta Explorer (Pharmacia Biotech). The SEC was conducted under a flow rate of 0.4 mL/min, a pressure limit of 1.5 mPa and an elution volume of 1 column volume with 500 μ L for each fraction.

4.4.3 PD10 buffer exchange

PD10 desalting columns contain sephadex g25 resin (Cytiva), which allows rapid group separation of high molecular weight molecules from low molecular weight molecules. PD10 desalting columns are used for desalting, buffer exchange and sample clean up. During gel filtration with PD10, small molecules like salts, free labels and other impurities are efficiently separated from the high molecular weight molecules of interest. First, the column was equilibrated with around 25 mL TEV-cleavage buffer or MSP storage buffer and the flowthrough was discarded. Afterwards, 2.5 mL sample was added to the column and flowthrough was discarded. Finally, 3.5 mL of TEV-cleavage buffer or MSP storage buffer were added and flowthrough was collected.

TEV-cleavage buffer

50 mM Tris-HCl, pH 8
25 mM NaCl
0.5 mM EDTA
2 mM DTT

MSP storage buffer

20 mM Tris-HCl, pH 7.4
150 mM NaCl
0.5 mM EDTA
5 mM sodium cholate

4.4.4 TEV-cleavage

N-terminal his-tags of MSPs were cleaved using TEV protease. TEV protease and MSPs were mixed in a 1:1 (w/w) ratio together with 0.5 mM EDTA and 2 mM DTT in TEV-cleavage buffer (see 4.4.3.). The mixture was incubated ON at 4 °C while shaking.

4.4.5 SDS-PAGE

Denatured proteins were separated through sodium dodecyl sulfate (SDS) polyacrylamide gel electrophoresis (PAGE). Proteins were separated according to their molecular weight since SDS is providing a negative net charge to the denatured proteins. Protein samples were mixed with 5x SDS sample buffer to prepare a 1x SDS-protein mixture and incubated for 15 - 20 min at 46 °C on a thermocycler. Samples were loaded onto a 5 % stacking gel with a pH of 6.8 to concentrate proteins before migrating into the separating gel with a higher pH of 8.8. In this thesis separation SDS gels were made using 30 % acrylamide solution diluted to concentrations of 15 %.

SDS-PAGE was performed in 1x Running buffer (freshly prepared from 10x running buffer stock) at 130 – 180 V/gel. The *BlueElf Prestained Protein Marker* (Jena Bioscience) was used as a reference for protein sizes. Polyacrylamide gels were incubated in Blue Silver stain over night at RT on a platform shaker to stain the proteins. Finally, Polyacrylamide gels were visualized using the ChemiDoc MP Imaging System (Biorad) and figures were prepared using PowerPoint.

5x SDS sample buffer	200 mM Tris-HCl (pH 6.8) 10 mM DTT 20 % Glycerol 10 % (w/v) SDS (Ultra Pure) 0.05 % (w/v) Bromphenol blue
Stacking gel (5 %)	17 % (v/v) Acrylamide 120 mM Tris/HCl (pH 6.8) 0.1 % (w/v) SDS 0.1 % (w/v) APS 0.1 % (v/v) TEMED 0.01 % (w/v) Bromphenol blue
Separating gel (15 %)	50 % (v/v) Acrylamide solution 250 mM Tris/HCl (pH 8.8) 0.1 % (w/v) SDS 0.1 % (w/v) APS 0.4 % (v/v) TEMED
10x Running buffer	250 mM Tris-Base 1920 mM Glycine 1 % (w/v) SDS (Pellets)
Blue silver stain	500 mL MilliQ® 10 % Phosphoric acid 10 % Ammoniumsulfate 1.2 % Coomassie G-250 Add MilliQ® to 800 mL 20 % Methanol

4.4.6 Western Blot analysis

Proteins separated from SDS-PAGE were transferred onto PVDF membranes (pore size 0.45 µm; Amersham) using the *Trans-Blot® Turbo™ Transfer System* (BioRad). PVDF membrane was activated by incubation in methanol for 10 min. Afterwards, polyacrylamide gels and PVDF membranes were soaked in Transfer buffer and placed between two blotting papers (Whatman) and put into a blotting cassette. Air-bubbles were removed carefully, the cassette was closed and placed into the *Trans-Blot®*

Turbo™ Transfer System. Blotting of proteins was performed at a continuous current of 25 V for 30 min.

After the complete protein transfer membranes were incubated in TBS-Tween (TBS-T) supplemented with 5 % non-fat dry milk for 20 min at RT on a platform shaker to block unspecific protein binding sites. Afterwards, anti his-tag antibody solution (Santa Cruz) was added and membranes were incubated overnight at 4 °C on a platform shaker. After incubation, antibody solution was removed and membranes were washed two times with TBS-T for 10 min and two times with TBS for 10 – 20 min. Membranes were incubated in 1:1 ratio of Chemiluminescent Solution 1 and Chemiluminescent Solution 2 and immediately visualized using the *ChemiDoc MP Imaging System* (Biorad). Figures were prepared using PowerPoint.

Transfer buffer	48 mM Tris-Base 39 mM Glycine 20 % (v/v) Methanol
10x TBS	46.2 mM Tris-Base 152.2 mM Tris-HCl 1.5 M NaCl
TBS-Tween	0.1 % (v/v) Tween 20 In 1x TBS
Chemiluminescent solution 1	5 ml 1 M TRIS Base, pH 8.5 220 µl p-Cumarinsäure 500 µl Luminol ad. to 50 ml with H ₂ O
Chemiluminescent solution 2	5 ml 1 M TRIS Base, pH 8.5 37 µl 30 % H ₂ O ₂ ad. to 50 ml with H ₂ O

4.5 Biophysical Methods

4.5.1 Circular dichroism and Fluorescence spectroscopy

Circular dichroism is used to rapidly determine the secondary structure and folding properties of proteins. It is defined as the unequal absorption of left-handed and right-handed circularly polarized light. A beam of light is polarized by passing through its electric field via suitable prisms or filters, leading to sinusoidally oscillation in a single plane. Molecules may absorb right- and left-handed circularly polarized light to different extents when interacting with such light. The result is a vector that traces out an ellipse and the light is said to be elliptically polarized, which can be illustrated by CD. Pooled

SEC fractions or single SEC fraction of choice was concentrated in 50 kDa centrifugal filters (Amicon[®], Merck) at 3900 xg to 60 μ L (Centrifuge 5804R, Eppendorf). Next, buffer was exchanged into CD buffer using *Zeba Spin 7K MWCO* desalting column (ThermoFischer). The sample was diluted to 220 μ L to a concentration of ca. 0.15 μ g/ μ L with CD Buffer. Circular dichroism (CD) and Fluorescence spectra (FL) were measured using *Aviv 420 Circular Dichroism Spectrometer* (Aviv, Biomedical Inc.) with fluorescence extension. CD and FL were measured at 4 °C and a wavelength of 190 nm – 260 nm for CD and 275 nm for tyrosine and tryptophane excitation and 295 nm for tryptophane excitation for FL spectroscopy. Figures were prepared using *Origin 2020* software (*OriginLab*).

To determine the concentration of Nsp6 and MSP2N2 in the Nsp-MSP2N2-POPC complex, densitometry analysis of SDS-PAGE was applied. A varied amount of MSP2N2 and BSA standard with known concentration determined by nanodrop was loaded on the same SDS-PAGE as Nsp6-MSP2N2-POPC complex. Using ImageLab software (BioRad), the intensity of Nsp6 and empty MSP2N2-POPC nanodiscs were determined. Empty MSP2N2-POPC sample was diluted to the calculated MSP concentration and CD and FL spectra was measured to subtract the contribution of MSP2N2 in the complex and thereby to obtain pure Nsp6 CD and FL spectra. Deconvolution of CD spectra was determined using BeStSel software.

4.5.2 Differential scanning fluorimetry

Differential scanning fluorimetry (DSF) is used to analyze the conformational stability and aggregation behavior of proteins under different thermal and chemical conditions. The conformational stability of a protein is described by its unfolding transition temperature, which can be measure at the point where half of the protein is unfolded. DSF monitors the intrinsic tryptophan fluorescence of proteins, which changes upon thermal unfolding. To evaluate the thermal protein stability of Nsp6 in MSP1E3D1-POPC nanodiscs, DSF using the inherent fluorescence of proteins (DSF) was used. The *Monolith NT.115 Premium Capillaries* (Nanotemper) was filled with protein sample prepared for CD/FL (see 4.5.5.) and placed on the sample holder. A temperature gradient of 1 °C per min from 15 °C to 95 °C was applied and the protein fluorescence at 330 nm and 350 nm was recorded using the *Nanotemper Prometheus NT.48 fluorimeter* (Nanotemper) controlled by *PR.ThermControl* (version 2.1.2). Figures were prepared using *Origin 2020* software (*OriginLab*).

4.5.3 Mass photometry

Molecular mass and oligomerization state of empty Nanodisc (MSP1E3D1-POPC) molecules and Nanodisc-Nsp6 complexes were determined using mass photometry. In principle, a single molecule exposed to a beam of light on a measurement surface produces a light scattering signal, which is directly proportional to the molecules mass. Previous to the measurement, ready-to-use sample carrier slides (Refeyn) covered by sample well cassette (Refeyn) were prepared and placed with some immersion oil onto the objective of the microscope of the photometer. The data was acquired using the *Refeyn TwoMP* mass photometer (Refeyn). Figures were prepared using *PhotoMol* software (spc.embl-hamburg.de).

4.5.4 Mass spectrometry

Molecular mass of MSP1E3D1 and Nsp6 was determined using matrix-assisted laser desorption/ionization (MALDI) mass spectrometry coupled with time-of-flight mass spectrometry (MALDI-TOF MS). Therefore, 1 μ L Protein standard II (Bruker LabScape-Daltonics) was mixed with 1 μ L 2 % trifluoroacetic acid-D (TFA) and 1 μ L 2,5-dihydroxy acetophenone + diammonium hydrogen citrate (matrix) and 0.5 μ L of the mixture was spotted on MTP targets steel plates (Bruker LabScape – Daltonics). Next, 2 μ L protein solution ($OD_{280} = 0.2$) was mixed with 1 μ L 2 % TFA and 1 μ L matrix and 0.5 μ L of the mixture was spotted on the same plate. Spotted sample mixtures were left to dry before measuring via *Autoflex[®] maX* (Bruker LabScape – Daltonics). Data acquisition was recorded using the *flexControl software* (Bruker) and data analysis was done using *flexAnalysis software* (Bruker).

5 Results

5.1 Preparation of relevant proteins

5.1.1 Generation (expression and purification) of TEV protease

Both the MSPs and the protein Nsp6 that was to be incorporated into the nanodiscs possess N-terminal his-tags. After in vitro expression of Nsp6 into nanodiscs, only nanodiscs containing Nsp6 should be separated via Ni-NTA affinity chromatography. Therefore, N-terminal his-tags from MSPs needs to be cleaved off to separate empty nanodiscs. For this reason, TEV protease was expressed and purified to cleave the his-tag from the MSPs.

TEV protease is a highly sequence-specific cysteine protease from Tobacco Etch Virus (TEV), which recognizes the amino acid sequence ENLYFQ/G and cleaves between Q and G [47]. This makes it attractive tools for removing affinity tags.

TEV protease was expressed in LB media using *E. coli* BL21 (DE) and purified using Ni-NTA resin. Due to the 6x His-tag, TEV has a molecular weight of around 28 kDa. As shown in Fig. 5, TEV protease was eluted using an imidazole gradient concentration of 100 – 750 mM in elution lanes 1 – 3, respectively. Furthermore, most of the TEV protease was eluted with an imidazole concentration of 300 mM (Fig. 5, elution lane 2).

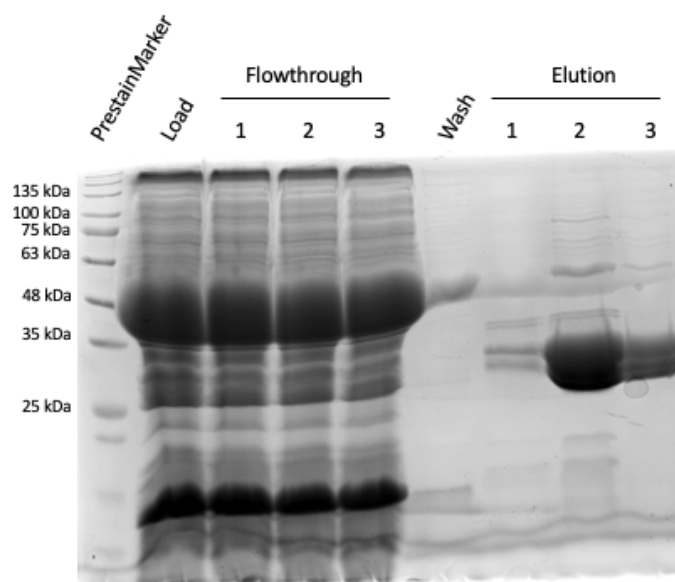


Figure 5: Coomassie stain of TEV protease purification steps. Purification was performed using Ni-NTA chromatography. TEV protease was eluted using 100 mM imidazole for elution 1 (lane 7), 300 mM imidazole for elution 2 (lane 8) and 750 mM imidazole for elution 3 (lane 9).

In the end, TEV purification yielded to a total protein yield of 3.5 mg/g cell pellet from a cell pellet yield of 16 g/L culture.

After purification, the optimal activity of TEV protease had to be explored to ensure the efficient cleavage of the His-tag from the MSPs. Therefore, three different ratios of TEV

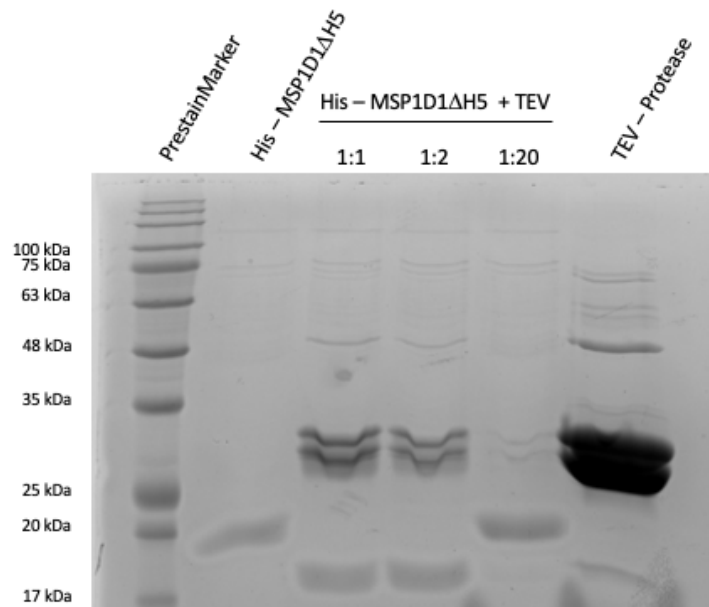


Figure 6: Coomassie stain of TEV protease activity test. Activity of TEV protease was verified by testing the cleavage of His-tag from MSP1D1 Δ H5 using three different (1:1, 1:2 and 1:20) ratios of TEV to MSP1D1 Δ H5.

to MSP (1:1, 1:2 and 1:20, w/w) were used to cleave His-MSP1D1 Δ H5 overnight at 4°C.

As seen in Fig. 6, lane 3 and 4, TEV was able to totally cleave His-tag from MSP1D1 Δ H5 in the ratios of 1:1 and 1:2, which leads to a decrease of molecular weight from 21 kDa to 19 kDa. In contrast, TEV was not able to totally cleave His-tag from MSP1D1 Δ H5 in a ratio of 1:20 (Fig. 6, lane 5).

5.1.2 Generation of MSPs

Membrane scaffold proteins are amphipathic proteins that are modified versions of apolipoprotein A1. MSPs are used for the formation of nanodiscs of different sizes. Nanodiscs are non-natural lipid bilayers composed of phospholipids surrounded by MSPs that are aligned in double belt formation to form a synthetic discoidal model membrane. Nanodiscs are able to incorporate and stabilize membrane proteins which retain them in a more native and soluble state compared to liposomes or detergents.

In this study, two different MSPs (MSP1E3D1 and MSP2N2) and POPC lipids were used for the assembly of nanodiscs.

5.1.2.1 Generation of MSP1E3D1

MSP1E3D1 is one of the smaller MSPs to use for nanodisc assembly. It exhibits a molecular weight of 29.98 kDa without His-tag and 32.6 kDa with His-tag on SDS-PAGE. In general, MSP1E3D1-POPC nanodiscs have a size of around 12-14 nm.

In this study, His-MSP1E3D1 was expressed using *E. coli* BL21(DE). Expressed MSP1E3D1 was purified using Ni-NTA resin and afterwards cleaved using TEV protease to remove the His-tag.

As seen in Fig. 7 A, lane 8, 32.6 kDa His-MSP1E3D1 was eluted using 500 mM Imidazole. Immediately after elution, His-tag was cleaved from MSP1E3D1 resulting in

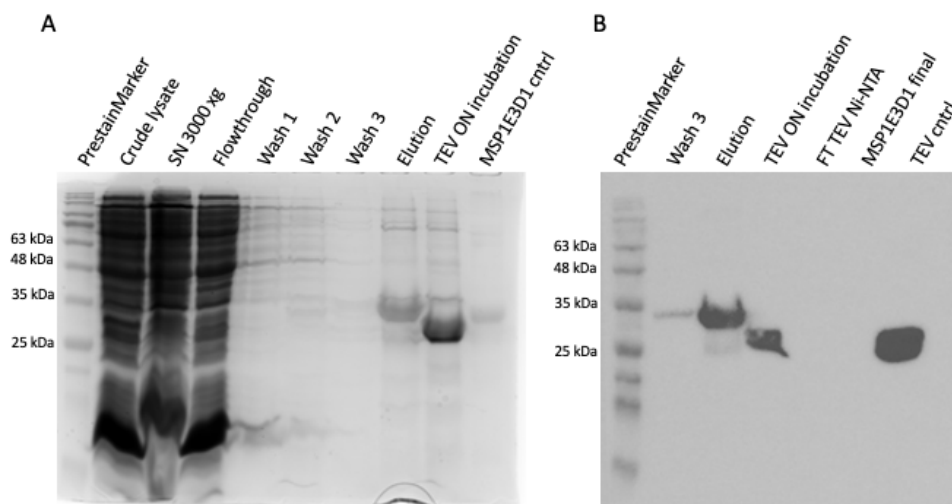


Figure 7: Analysis of MSP1E3D1 purification steps and TEV cleavage by Coomassie stain and Western Blot. Purification was performed using Ni-NTA chromatography and 32.6 kDa His-MSP1E3D1 and 29.98 kDa MSP1E3D1 were expected. A) Coomassie stain of MSP1E3D1 purification steps showing the elution of His-MSP1E3D1 using 500 mM Imidazole (lane 8) and the removal of His-tag using TEV protease (lane 9). B) Verification of TEV protease cleavage by Western Blot showing no His-tag signal after TEV cleavage and TEV removal by Ni-NTA chromatography (lane 5 – 6).

29.98 kDa MSP1E3D1 (Fig. 7 A, lane 9). To ensure the removal of His-tag from MSP1E3D1, western blot using His-antibodies was performed. In Fig. 7 B, no signal appears in lane 5 and 6 in contrast to the elution of purified MSP1E3D1 in lane 3, verifying the removal of His-tag from MSP1E3D1. After TEV cleavage of MSP1E3D1, a total cell pellet yield of 16.9 g/L culture was achieved. Total protein yield of MSP1E3D1 was 2.9 mg/g cell pellet.

5.1.2.2 Generation of MSP2N2

In contrast to MSP1E3D1, MSP2N2 is larger in size showing a molecular weight of 45.67 kDa with His-tag and 43.05 kDa without His-tag. Assembled MSP2N2-POPC nanodiscs show a size of 17 nm. The larger diameter may allow Nsp6 to adopt higher oligomerization state.

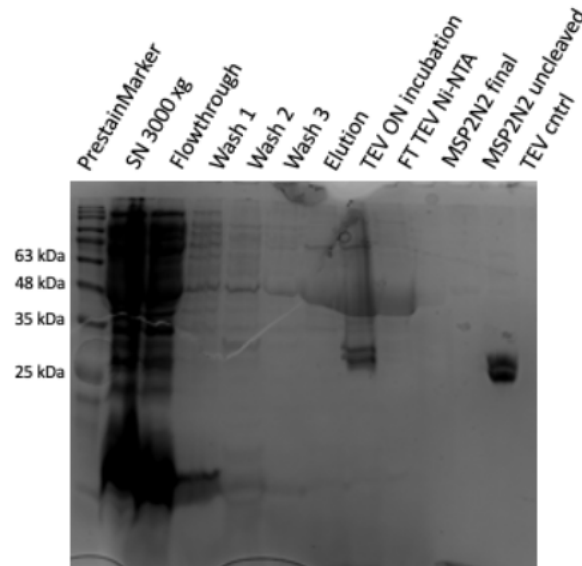


Figure 8: Coomassie stain of MSP2N2 purification steps. Purification was performed using Ni-NTA chromatography and 45.67 kDa His-MSP2N2 and 43.05 kDa MSP2N2 were expected. The elution of His-MSP2N2 using 500 mM Imidazole can be seen in lane 7 and the removal of His-tag using TEV protease is shown in lanes 8 – 10.

Similar to MSP1E3D1, MSP2N2 was expressed using *E. coli* BL21(DE) and purified using Ni-NTA resin and afterwards cleaved using TEV protease to remove the His-tag. In Fig. 8, lane 7 45.67 kDa His-MSP2N2 was eluted using 500 mM Imidazole. Immediately after purification, His-tag was cleaved from MSP2N2 using TEV protease resulting in 43.05 kDa MSP2N2 as seen in Fig. 8, lane 8 – 10). Finally, a total cell pellet yield of 15.1 g/L culture of MSP2N2 and total protein yield of 2.18 mg/g cell pellet was achieved.

5.1.3 Nanodisc assembly with different MSPs

Membrane proteins are proteins associated or attached to the membrane of a cell or the membrane of cellular organelles. Together with hydrophilic extra- and intracellular domains, the majority of membrane proteins show an amphipathic character, which makes it difficult to analyze them in their native environment. Membrane proteins are unstable in standard aqueous buffers, which precludes detailed characterization of many membrane proteins. However, nanodiscs provide an alternative for the

stabilization of different membrane proteins by mimicking the amphipathic environment of a lipid bilayer and thus, allow maintaining a physiologically relevant state of the membrane protein structure. In general, nanodiscs are composed of two membrane scaffold proteins, which wrap around lipids forming a disc-like particle. In this study, the two different nanodiscs composed of MSP1E3D1 and MSP2N2 scaffold proteins and POPC lipids are used to stabilize Nsp6 protein. Scaffold proteins and lipids are combined during the self-assembly process. This process depends on different buffer components, temperature pH and the membrane scaffold protein to lipid ratio. After the self-assembly process, SEC was performed to sort sample molecules according to their size. A homogeneous sample was obtained by selecting the central peak fractions for further work.

SEC profiles of assembled nanodiscs show the successful production of MSP1E3D1-DMPC/POPC nanodiscs as seen in Fig.9 A/B. Both SEC profiles exhibit large elution peaks at 17.08 mL and 17.1 mL for MSP1E3D1-POPC and MSP1E3D1-DMPC, respectively. Using SEC calibration curve a size of around 150-200 kDa for both nanodiscs was determined. In Fig.9 D, a successful production of MSP2N2-POPC nanodiscs is shown with an elution volume of 15.5 mL at the major peak corresponding to a size of 400 kDa according to SEC calibration curve, whereas the production of MSP2N2-DMPC did not work as seen in Fig.9 C. Besides, major peak fractions were tested via SDS-PAGE to see whether the eluted nanodiscs are homogeneous in molecular weight.

As seen in Fig. 9 E - F, MSP1E3D1-POPC/DMPC nanodiscs show some impurities. Beside the 29 kDa MSP1E3D1 other molecules with a size of 48 kDa, 70 kDa and higher were detected by SDS-PAGE. However, both nanodiscs have their major peak at fraction C3 with highest homogeneity. In contrast, elutions of MSP2N2-POPC and MSP2N2-DMPC do not show any impurities in SDS-PAGE. In addition, MSP2N2-POPC nanodiscs seem to have their major peak at fractions from B11 - C1. However, MSP2N2-DMPC elution does not show major peak fractions since every protein band show the same intensity in SDS-PAGE. In addition, overlapping of several elution peaks was detected from the SEC.

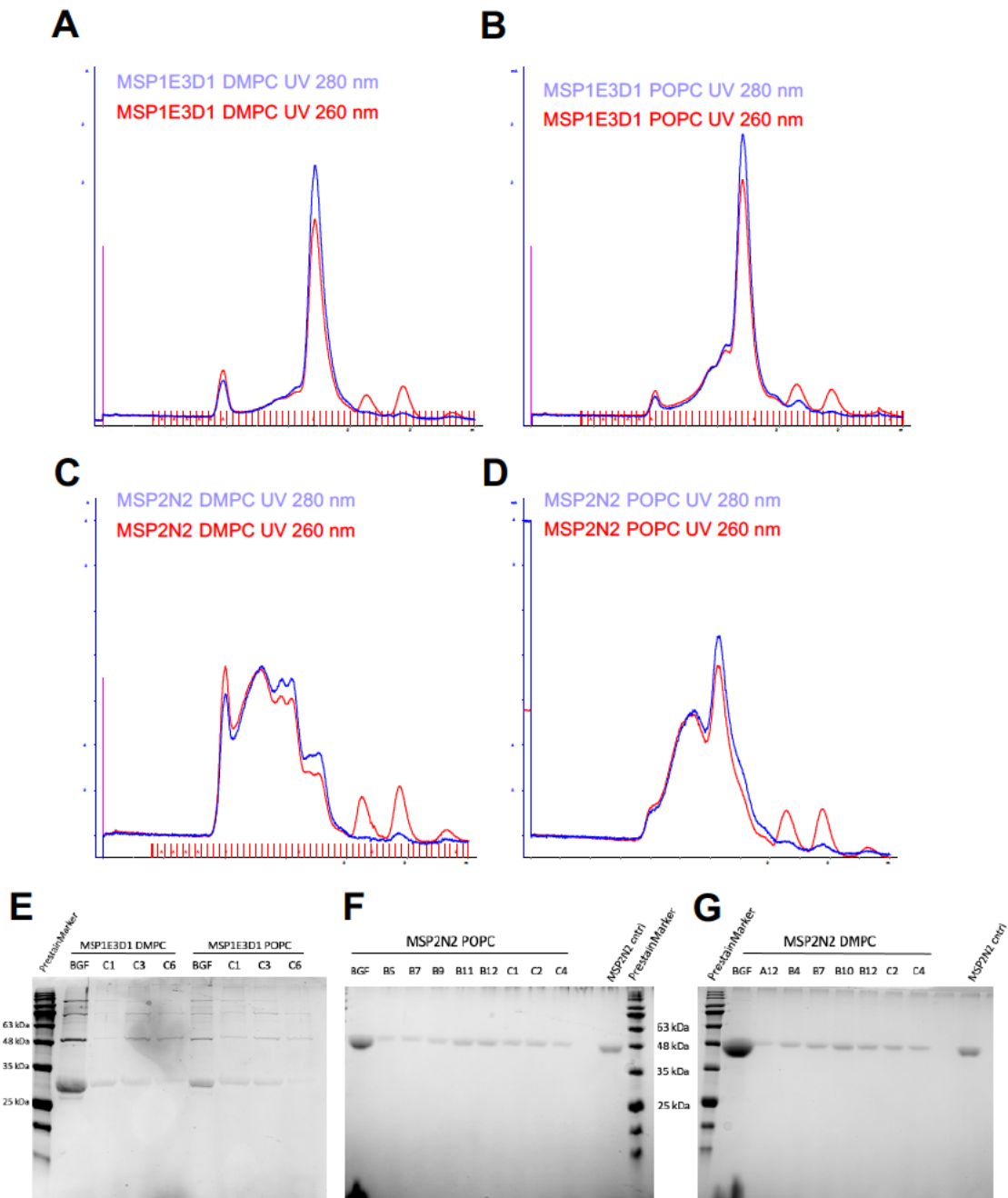


Figure 9: Analysis of different assembled nanodiscs. Second purification of different nanodiscs was performed using size exclusion chromatography. A-D are showing the different SEC profiles of each nanodisc. E-G) SEC fractions were pooled, separated via SDS-PAGE and analyzed with Coomassie stain.

5.2 Generation of Nsp6-Nanodisc-complexes

The expression of membrane proteins like Nsp6 is often challenging since membrane proteins are highly unstable in aqueous solutions. As an alternative to often used detergents to stabilize or solubilize membrane proteins, nanodiscs were used in this work. For the expression of Nsp6 in nanodiscs, an *in vitro* system expressing Nsp6 using *E. coli* lysate containing T7 RNA polymerase enzyme was used. Further components were reaction buffer, protease inhibitors, IPTG, nanodiscs and Nsp6

plasmid. After incubation and ultracentrifugation, purification of His-tagged Nsp6-nanodisc-complexes was performed using Ni-NTA resin.

Purification steps were analyzed using western blot analysis and SDS-PAGE as seen in Fig. 10. Western Blot analysis of washing steps during purification is Fig. 10 A shows very high His-tag signals at 25 kDa, 30 kDa and 60 kDa with the load in lane 1. In contrast, a lot of signals are seen in Fig. 10 B with load and flowthrough in the SDS-PAGE as well as a signal at MSP1E3D1 control. However, western blot analysis of elution steps 1 - 5 display His-tag signals at 30 kDa in all elution steps and some additional signals at 25 kDa and 60 kDa with elution steps 1 - 3 and no signal with MSP1E3D1 control (Fig. 10 C). Likewise, SDS-PAGE analysis in Fig. 10 D shows high signals at 30 kDa in every elution step and some additional signals at 25 kDa, 50 kDa, 60 kDa and 70 kDa and also a very high signal with MSP1E3D1 control. Nsp6 has a theoretically molecular weight of around 34 kDa but according to western blot analysis it seems to run in SDS-PAGE at around 30 kDa, which is most often the case for membrane proteins due to presence of bound detergents, lipids or unusual amounts of bound SDS.

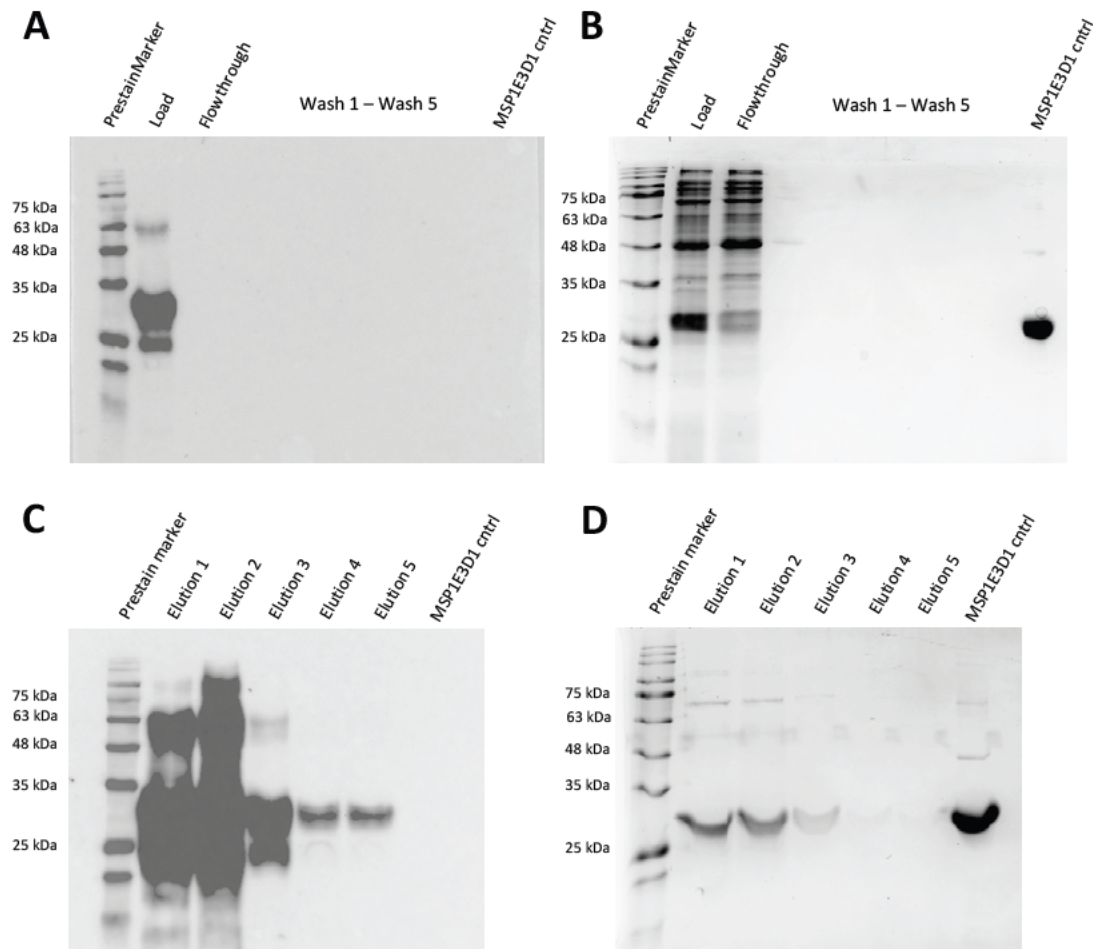


Figure 10: Western Blot analysis and Coomassie stain of purification steps of Nsp6-MSP1E3D1-POPC complexes. Purification was performed using Ni-NTA Indigo chromatography and 34 kDa Nsp6 and 29 kDa MSP1E3D1 were expected to elute on steps of Coomassie stain and on Nsp6 Western blot analysis. A) Western blot of purification wash steps. B) Coomassie stain of purification wash steps. C) Western blot analysis of purification elution steps. D) Coomassie stain of purification elution steps. Proteins were detected using antibody specific for His-tag.

After purification via Ni-NTA, elution steps were pooled, concentrated and again purified according to size via SEC.

SEC profile of Nsp6 in MSP1E3D1-POPC shows an elution peak of around 17.4 mL as seen in Fig. 11 A. SEC profile of Nsp6 in MSP2N2-POPC shows an elution peak of around 16.1 mL which is smaller compared to empty MSP2N2-POC with an elution peak of around 15.5 mL as seen in Fig. 11 B. The smaller elution volume may be due to the fact that the insertion of Nsp6 replaces many lipid molecules.

Likewise, SDS-PAGE analysis of MSP1E3D1-POPC nanodiscs containing Nsp6 revealed bands of around 30 kDa in mass (Fig. 11. C) in which the bands in fraction B12, C2 and C4 are more intense than other bands, overlapping with the MSP1E3D1 protein. Since MSP1E3D1 and Nsp6 both show a similar apparent molecular weight

of 30 kDa (Nsp6 in theory 34 kDa) in SDS-PAGE analysis, they seem to overlap and to be difficult to distinguish. In contrast, SDS-PAGE analysis of Nsp6 in MSP2N2-POPC nanodiscs shows two major bands at 30 kDa for Nsp6 and 48 kDa for MSP2N2 in which fractions B12 and C1 are more intense and seems to contain most of the protein. In conclusion, the presence of Nsp6 could be verified in both nanodiscs via SDS-PAGE and western blot analysis after SEC purification with an apparent molecular weight of 194 kDa at a yield of 0.22 mg/ml *in vitro* cell lysate.

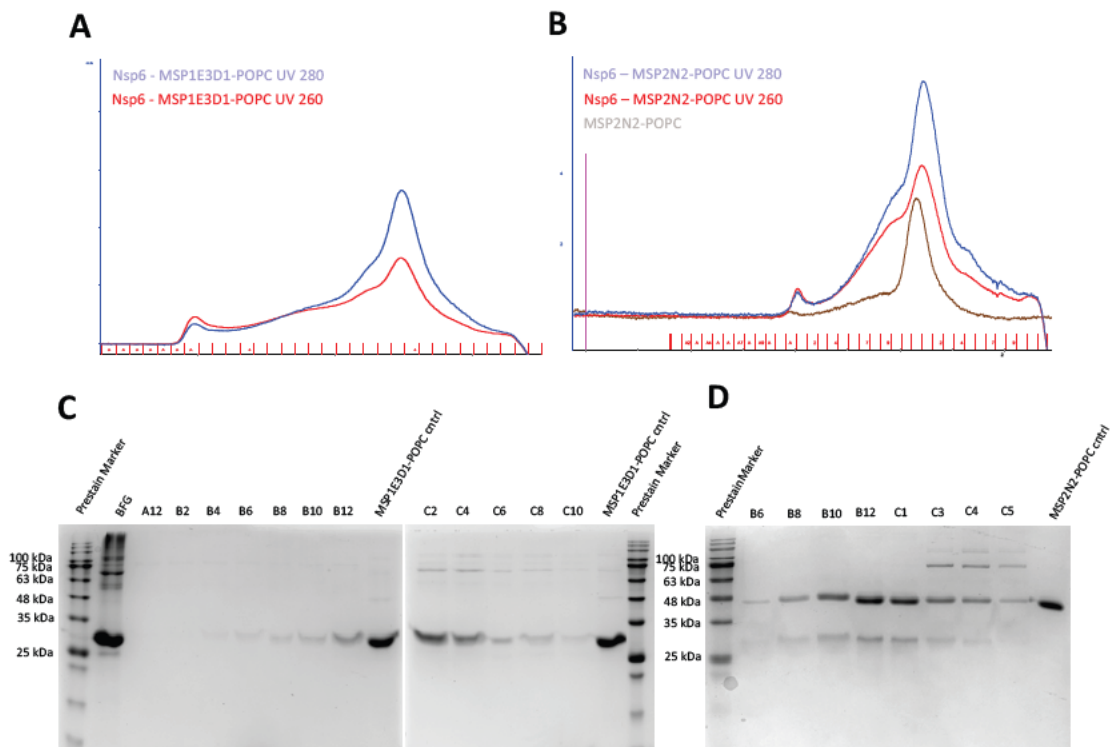


Figure 11: Analysis of different Nsp6-nanodisc-complexes via SEC and SDS-PAGE. Second purification of Nsp6 in MSP1E3D1-POPC and MSP2N2-POPC nanodiscs was performed using size exclusion chromatography. A-B) Different SEC profiles of each Nsp6-nanodisc complex. C-D) SEC fractions of peaks were pooled, separated via SDS-PAGE and analyzed with Coomassie staining.

5.3 Biophysical characterization of Nsp6 and Nsp6-Nanodisc-complexes

After expression and purification of Nsp6 in different nanodiscs, several structure properties have to be analyzed. Primary, secondary as well as tertiary structure can be characterized or accessed using different biophysical methods.

5.3.1 Analysis of the primary structure of Nsp6 and Nsp6-MSP1E3D1-POPC complexes

5.3.1.1 Investigation of the molecular masses of Nsp6 and MSP1E3D1 via mass spectrometry

To analyze the molecular mass by mass spectrometry, MALDI-TOF (matrix assisted laser desorption ionization – time of flight) MS was used. MALDI is a soft ionization that strikes a molecule containing matrix to put the molecules into the gas phase without decomposing. Molecular masses of ionized molecules are measured using TOF principle. Here, ions of different mass to charge ratios (m/z) need different times to flight along a field-free drift path of known length, which leads lighter molecules to arrive earlier at the detector than heavier ones.

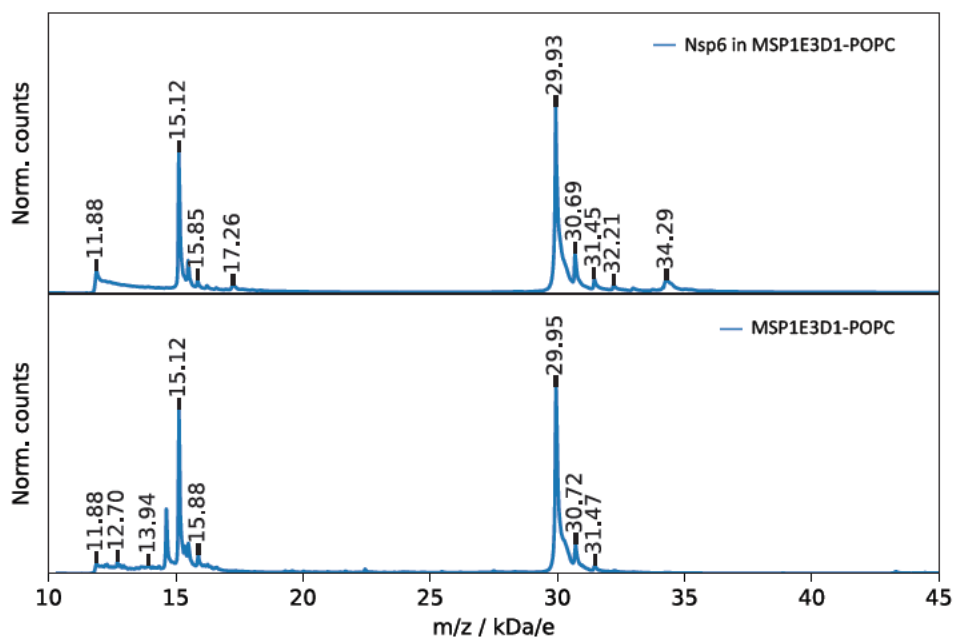


Figure 12: Mass spectrometry analysis of Nsp6 in MSP1E3D1-POPC and of empty MSP1E3D1-POPC nanodiscs using MALDI-TOF MS. MALDI mass spectrum of Nsp6-MSP1E3D1-POPC complexes in the upper part and MALDI mass spectrum of empty MSP1E3D1-POPC nanodiscs in the lower part of the image.

Mass spectrometry analysis of empty MSP1E3D1-POPC nanodiscs show sharp signals at 29.95 kDa/e, 30.72 kDa/e and 31.47 kDa/e as seen in the lower part of Fig. 12. The mass 29.95 kDa/e corresponds to the scaffold protein MSP1E3D1,

whereas the remaining peaks may be due to binding of POPC lipid molecules. On the other side, mass spectrometry analysis of Nsp6 in MSP1E3D1-POPC nanodiscs reveals signals at 29.93 kDa/e, 30.69 kDa/e, 31.45 kDa/e, 32.21 kDa/e and 34.29 kDa/e as seen of the upper part of Fig. 12. The mass 34.29 kDa/e corresponds to the Nsp6 protein and the mass 29.93 kDa/e corresponds to the scaffold protein equally to the 29.95 kDa/e in the mass spectrometry analysis of empty nanodiscs.

5.3.1.2 Investigation of molecular mass of Nsp6-MSP1E3D1-POPC complexes via mass photometry

Molecular mass and oligomerization state was analyzed using mass photometry system. While a single molecule strikes a measurement surface which is exposed to a beam light, the molecule produces a measurable light scattering signal. The signal directly proportional to the molecules mass.

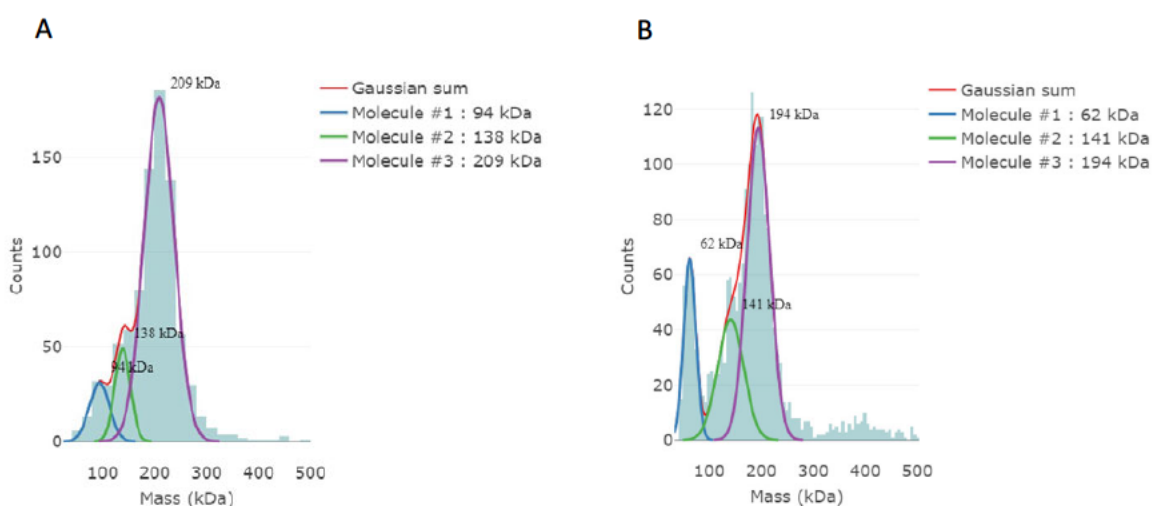


Figure 13: Mass photometry analysis of MSP1E3D1-POPC and Nsp6-MSP1E3D1-POPC complexes. The mass photometry histogram presents the data as a histogram and the peaks are fitted by Gaussian curves. A) Histogram of mass photometry analysis of empty MSP1E3D1-POPC nanodiscs. B) Histogram of mass photometry analysis of Nsp6-MSP1E3D1-POPC complexes.

Mass photometry analysis data of empty MSP1E3D1-POPC nanodiscs is plotted in the histogram in Fig. 14 A. Each peak is fitted by a gaussian curve. The first peaks show molecules of 94 kDa and 138 kDa. The most dominant peak with the highest counts shows a molecular mass of 209 kDa which fits the theoretical molecular mass of MSP1E3D1-POPC empty nanodiscs. Besides, mass photometry analysis data of Nsp6-MSP1E3D1-POPC complexes is plotted in the histogram in Fig. 14 B, also showing two smaller molecules with a molecular mass of 62 kDa and 141 kDa and a

larger molecule with over 100 counts of 194 kDa. However, the 194 kDa molecule fits the Nsp6-MSP1E3D1-POPC complex best.

5.3.1.3 Analysis of the thermal stability of MSP1E3D1-POPC and

Nsp6-MSP1E3D1-POPC complexes via differential scanning fluorimetry

To measure the thermal unfolding of Nsp6 and Nsp6-MSP1E3D1-POPC complexes under label-free, native conditions by detecting changes in its intrinsic fluorescence during a thermal gradient, differential scanning fluorimetry (DSF) was applied.

The melting curves of empty MSP1E3D1-POPC nanodiscs show a negative peak around 55 °C and a positive peak around 90 °C, whereas the melting curves of Nsp-MSP1E3D1-POPC shows two negative peaks around 55 °C and 70 °C (Fig. 14). Since the negative peak around 55 °C appears for both the Nsp6-MSP1E3D1-POPC and the MSP1E3D1-POPC melting curves, it probably belongs to melting of the MSP1E3D1-POPC. The positive peak around 90 °C could come from lipids. The second negative peak around 70 °C of the Nsp6-MSP1E3D1-POPC melting curve may come from Nsp6. However, melting curves do not give a typical two state structure transitions upon thermal unfolding.

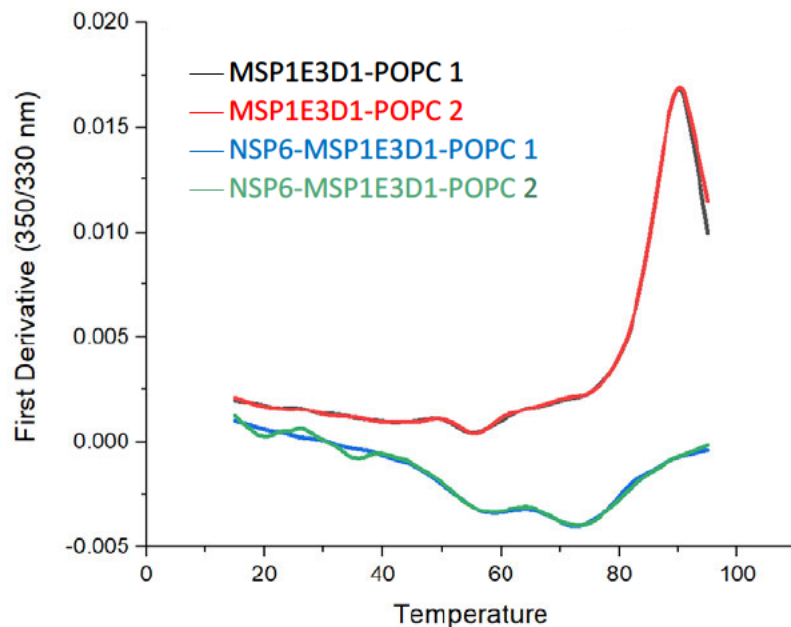


Figure 14: Differential scanning fluorimetry analysis of the thermal stability of Nsp6-MSP1E3D1-POPC complexes and MSP1E3D1-POC. Detection of DSF signals for MSP1E3D1 and Nsp6-MSP1E3D1 complexes by heating from 15 °C to 95 °C with a ramp rate of 1 °C/min. Fluorescence emission at 330 nm and 350 nm were measured and first derivative of division of the 350 nm signal by the 330 nm signal was illustrated.

5.3.2 Analysis of secondary structure of Nsp6-nanodisc complexes via circular dichroism

The secondary structure of proteins can be determined using circular dichroism (CD) spectroscopy. Predicted three-dimensional structure model of Nsp6 by AlphaFold consists of seven transmembrane alpha-helices (Fig. 15 A) [47]. CD analysis of Nsp6 sample in MSP1E3D1-POPC nanodiscs, measured at 4 °C display a far UV spectra, characterized by two minima at 222 nm and 209 nm and a positive ellipticity at 193 nm, typical for alpha-helices as seen in Fig. 15 B and C. These results are in agreement with the model predicted by AlphaFold.

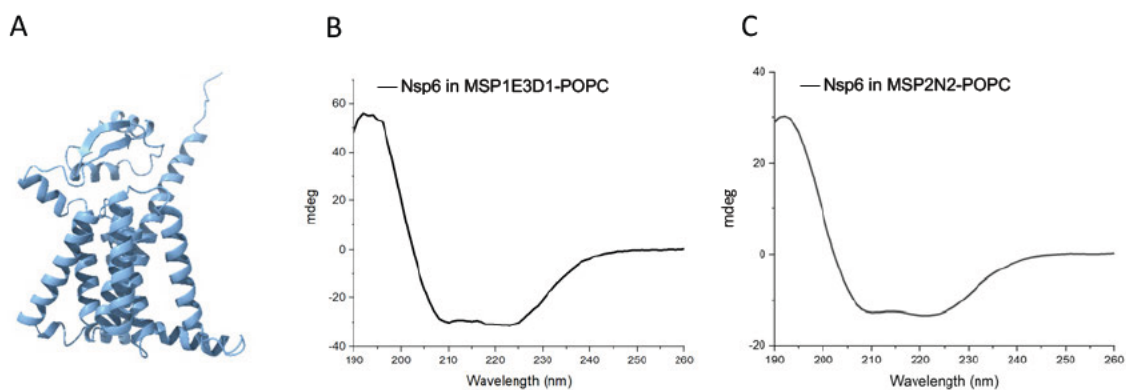


Figure 15: Circular dichroism spectroscopy analysis of Nsp6-nanodisc complexes. A) AlphaFold model of Nsp6. B) CD spectra of Nsp6-MSP1E3D1-POPC complex, showing a characteristic alpha-helical structure. C) CD spectra of Nsp6-MSP2N2-POPC complex, showing a characteristic alpha-helical structure.

Similar to CD analysis of Nsp6 sample in MSP1E3D1-POPC nanodiscs, Nsp6 in MSP2N2-POPC sample shows two minima at 222 nm and 209 nm and a positive ellipticity at 193 nm, which is typical for alpha-helices (Fig. 15 C).

5.3.2.1 Analysis of secondary structure of Nsp6

To probe pure Nsp6 secondary structure in Nsp6-MSP1E3D1-POPC complex, densitometry analysis of protein bands from SDS-PAGE was applied to determine the intensity of Nsp6 and MSP in the complex. Since MSP1E3D1 and Nsp6 are difficult to distinguish in SDS-PAGE analysis, MSP2N2 was used for the deconvolution. Using calibration curves of BSA standard and MSP2N2, the concentration of MSP2N2 and Nsp6 was calculated (Fig. 16).

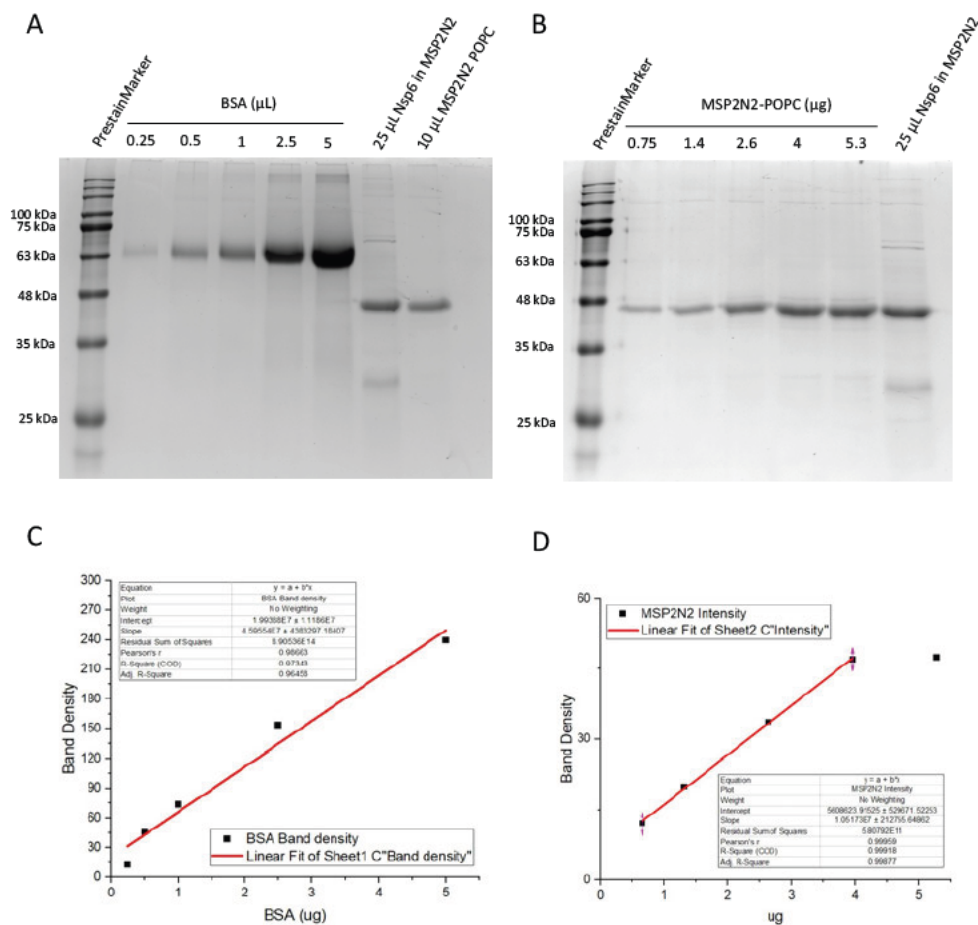


Figure 16: SDS-PAGE for densitometry analysis of BSA standard and MSP2N2-POPC and its calibration curves. A) SDS-PAGE oaded w th known concentrat ons of BSA standard, known vo ume of Nsp6-MSP2N2-POPC comp ex and MSP2N2-POPC. B) SDS-PAGE oaded w th known concentrat ons of MSP2N2-POPC and known vo ume of Nsp6-MSP2N2-POPC comp ex. C) Ca brat on curve of BSA standard us ng dens tometry ana ys s of SDS-PAGE. D) Ca brat on curve of MSP2N2-POPC us ng dens tometry ana ys s of SDS-PAGE. Ca brat on curves were used to ca cu ate the concentrat on of MSP2N2-POPC and Nsp6 n Nsp6-MSP2N2-POPC comp ex.

After determining the exact concentration of MSP2N2, CD spectra of MSP2N2 nanodiscs at the specific concentration were measured. As seen in Fig. 17, CD spectra of Nsp6-MSP2N2-POC complexes and MSP2N2-POPC alone were measured. Afterwards, CD spectra of MSP2N2 was subtracted from CD spectra of Nsp6-MSP2N2-POPC complex, giving the CD spectra of Nsp6 alone. CD spectra of Nsp6 alone shows two minima at 222 nm and 209 nm and a maximum at 193 nm, typical for alpha helical structures. After deconvolution, CD spectra of Nsp6 exhibit 74.7 % helical structures, from which 50.7 % were regular and 24 % were distorted helical structures. Besides, 5.5 % of turn and 19.8 % of other structures were identified (Table 1). In Table 2, deconvolution of MSP2N2 spectra determined 11.5 % alpha helical structures, 41 % Antiparallel, 13.3 % turn and 34.2 % other structures. Furthermore, deconvolution of CD spectra of Nsp6-MSP2N2 complexes revealed

41.9 % of alpha helices, 28.3 % antiparallel, 13.7 % of turn and 16.1 % of other structures as seen in Table 3.

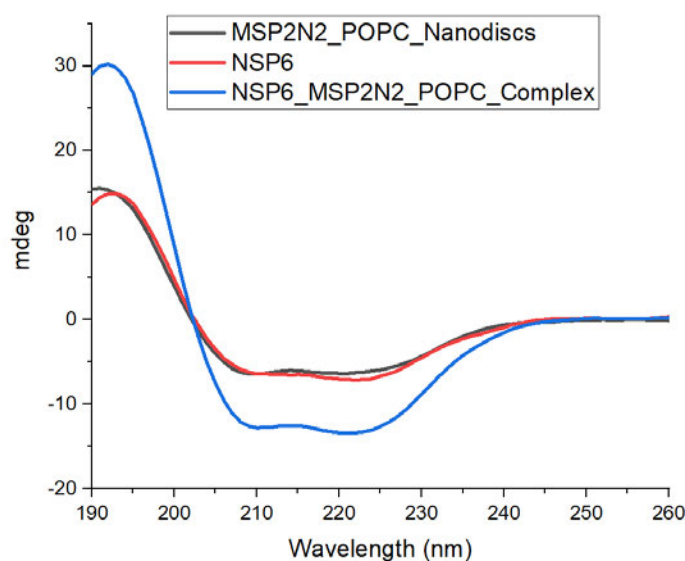


Figure 17: CD spectra of Nsp6-MSP2N2-POPC, MSP2N2-POPC and Nsp6 after deconvolution. After densitometry analysis of SDS-PAGE and calculation of MSP2N2-POPC concentration using calibration curves, CD spectra of MSP2N2-POPC (black) was subtracted from Nsp6-MSP2N2-POPC (blue) CD spectra to obtain CD spectra of Nsp6 alone (red). CD spectra of Nsp6 shows typical alpha helix structure features.

Table 1: Estimated secondary structure content of Nsp6

Helix	74.7 %	Antiparallel	0.0 %
Helix1 (regular)	50.7 %	Parallel	0.0 %
Helix 2 (distorted)	24.0 %	Turn	5.5 %
		Others	19.8 %

Table 2: Estimated secondary structure content of MSP2N2-POPC

Helix	11.5 %	Antiparallel	41 %
Helix1 (regular)	9.8 %	Parallel	0.0 %
Helix 2 (distorted)	1.7 %	Turn	13.3 %
		Others	34.2 %

Table 3: Estimated secondary structure content of Nsp6-MSP2N2-POPC complex

Helix	41.9 %	Antiparallel	28.3 %
Helix1 (regular)	33.7 %	Parallel	0.0 %
Helix 2 (distorted)	8.2 %	Turn	13.7 %
		Others	16.1 %

5.3.3 Analysis of tertiary structure of Nsp6 and Nsp6-nanodisc complexes via fluorescence spectroscopy

To probe the tertiary structure of Nsp6 in nanodiscs, fluorescence (FL) spectroscopy was applied. Tryptophan in solution displays an excitation maximum near 280 nm and emits near 350 nm when measured at a wavelength of 295 nm. However, to get the FL spectra of Nsp6 alone, FL of Nsp6-MSP2N2-POPC complex and of MSP2N2-POPC were measured and FL spectra of MSP2N2-POPC was subtracted from FL spectra of the complex as seen in Fig. 18 A and B. Emission λ_{\max} of tryptophane of Nsp6 alone was obtained at 335 nm, which is 15 nm lower than for free tryptophan suggesting an average of buried tryptophan (Fig. 18 B). Tyrosine fluorescence will be quenched when the distance between tyrosine and tryptophan is

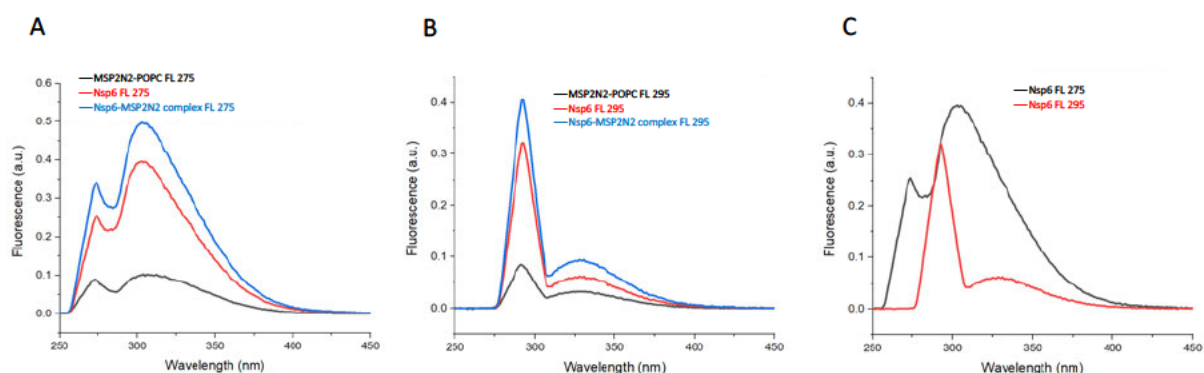


Figure 18: Fluorescence spectra of MSP2N2-POPC, Nsp6-MSP2N2-POPC and Nsp6. A) Fluorescence measured at 275 nm for tryptophan and tyrosine. **B)** Fluorescence measured at 295 nm for tryptophan. **C)** Fluorescence spectra of Nsp6 measured at 275 nm and 295 nm.

within the FRET distance. FL spectra of tryptophan and tyrosine mixture compared to the FL spectra of tryptophan alone showed a higher fluorescence intensity for Nsp6. The higher fluorescence intensity of tyrosine and tryptophane implies in a low FRET (föster resonance emission transfer), which means that there is a high average distance between tryptophan and tyrosine in the protein structure (Fig. 18 C). The distance between tryptophan and tyrosine in MSP2N2 is shorter compared to Nsp6, since fluorescence intensity measured at 275 nm is almost the same as for 295 nm wavelength.

6 Discussion

In this study, two different nanodiscs MSP1E3D1-POPC and MSP2N2-POPC were assembled. Recent studies reported that Nsp6 undergoes homodimerization, which is required to generate the NSP6 compartment [48]. Therefore, different sizes of nanodiscs, especially nanodiscs of bigger size were used in this work. The diameter of the nanodiscs could have an effect on the oligomerization state of Nsp6. Prior to this work, Nsp6 was expressed *in vitro* using MSP1D1 Δ H5-POPC nanodiscs which are around 7-8 nm. Results of SEC reveals several peaks, indicating non-homogeneous Nsp6-nanodisc complexes (results not shown). Hence, nanodiscs of bigger size of 12 and 17 nm (MSP1E3D1-POPC/MSP2N2-POPC) were chosen to allow proper oligomerization of Nsp6. Besides, two kinds of lipids with different transition temperatures (4 °C for POPC and 25 °C for DMPC) were tested before up-scale *in vitro* expression of Nsp6.

As seen in Fig. 9, nanodiscs containing POPC lipids run more homogeneous in SEC. Since a lower transition temperature of native lipids results in a more fluid lipidic nanodiscs, MSP1E3D1-POPC lipids seem to be more stable, which lead to the decision to use POPC lipids for the assembly of the different nanodiscs.

In the context of this work, Nsp6 was successfully expressed *in vitro* using nanodiscs of different sizes, allowing the characterization of the primary, secondary and tertiary structure of Nsp6 via different biophysical methods.

Mass spectrometry analysis of NSP6-MSP1E3D1-POPC complexes and empty MSP1E3D1-POPC nanodiscs using MALDI-TOF revealed signals of around 29.9 kDa with a high number of counts (Fig. 12). This peak corresponds to the molecular weight of the MSP1E3D1. On the contrary, mass spectrometry analysis of Nsp6-SMSP1E3D1-POPC complexes revealed a low signal of around 34.29 kDa, which corresponds to the size of the Nsp6 protein. The theoretically calculated molecular weight of Nsp6 was 34,27 kDa, which indicates that the purified protein is complete. However, the number of counts for the Nsp6 signal is considerably low in comparison to the MSP1E3D1 signal. Notably, not all peptides “fly” in the mass spectrometer. On the one hand, molecules can fail to ionize, on the other hand, some ions are too unstable and can fragmentate during ionization, leading them not to be

detectable. Besides, some samples are simply not ionizable in the matrix mixture and does not “fly” to the detector [49][50].

Analysis of mass photometry revealed two major peaks of 209 kDa for empty MSP1E3D1-POPC nanodiscs and 194 kDa for Nsp6-MSP1E3D1-POPC complexes. Since the light scattered by the molecules measured via mass photometry is proportional to the molecular mass, these results suggest higher molecular weight of MSP1E3D1-POPC empty nanodiscs than Nsp6-MSP1E3D1-POPC complexes, claiming that there is one Nsp6 protein incorporated in each nanodisc. An explanation for this could be that the amount of lipid molecules needed to be replaced by Nsp6 after incorporation have a higher molecular weight than the protein itself. Besides, additional peaks at 62 kDa and 94 kDa appear in the mass photometry histogram, which probably come from different impurities in the buffer [51], whereas further peaks around 140 kDa could come from free lipid particles floating around in the sample.

Dynamical protein motions are required for functional activity. Interestingly, dynamic transitions of protein motions are temperature-dependent, leading temperature to be a potential probe for the functional role of such motions [52]. However, not all motions in proteins are sensitive to temperature in the same way. Differential scanning fluorimetry analysis of MSP1E3D1-POPC nanodiscs measured as the minimum of the first derivative revealed a melting temperature of around 55 °C for nanodiscs and a second peak around 90 °C which could come from free lipids. Likewise, DSF analysis of Nsp6-MSP1E3D1-POPC complexes measured as the minimum of the first derivative showed the same peak around 55 °C for the nanodiscs with an additional peak probably coming from Nsp6. To ensure that the melting curve with the peak around 55 °C comes from MSP1E3D1, DSF analysis of MSP1E3D1 alone should be detected. Additionally, DSF melting curve of POPC lipids could be investigated to prove the peak around 90 °C comes from lipid molecules. However, both melting curves do not give typical transition temperature peaks. In the case of Nsp6, its structure could be rigid, which makes it resistant against unfolding. Besides, the unfolding process of Nsp6 could be accompanied by aggregation which may disturb the thermal unfolding process.

Far-UV CD detected the spectrum typical for helical protein. Deconvolution after subtraction of purified Nsp6 showed 75 % alpha helical secondary structure content (Table 1). The alpha-fold model predicts 74 % helical and 4 % beta-structure, which is broadly in agreement with the experimental data. However, further deconvolution of CD spectra of MSP2N2-POPC and Nsp6-MSP2N2-POPC complexes revealed less alpha helical structures than expected. Since the BeStSel software relies on datasets derived from a database, the most similar structures are compared to the measured CD dataset to find out their fold classification. This means, that there may be no comparable structure in the database for the MSP2N2 protein, which leads to a different deconvolution and structure composition than expected. Moreover, the ratio of Nsp6 to MSP2N2 per nanodisc was estimated to be 1:2. That means, two MSP2N2 proteins and one Nsp6 per nanodisc, which fits the experimental data perfectly.

Protein tryptophan fluorescence maximum peak occurred at ~335 nm for purified Nsp6. Since tryptophan fluorophores inside the protein in a low-polar hydrophobic environment shows with a shorter-wavelength position an emission maximum around 330 nm, emission maximum of Nsp6 at 335 nm (Fig. 18 C) is typical for the buried hydrophobic microenvironment of tryptophan side chains [53]. Moreover, buried tryptophan further indicates a proper folded tertiary structure of Nsp6.

In a compact protein structure, protein tyrosine fluorescence is not detectable, due to higher absorption coefficients and quantum yields of tryptophan residues and the Förster resonance energy transfer (FRET) from tyrosine to tryptophan [54]. When within the FRET distance, tryptophan quenches tyrosine emission, resulting the tryptophan as the most reliable residue for FRET [55]. The absorption of tryptophan is several times larger than tyrosine absorption at all wavelengths. As seen in Fig. 18 C, a higher fluorescence intensity of tyrosine and tryptophan compared to tryptophan fluorescence intensity, prove that not all tyrosine fluorescence is quenched by tryptophan, suggesting a high average distance between tryptophan and tyrosine in the protein structure.

In conclusion, *in vitro* expression and two-step purification of Nsp6-MSP1E3D1-POPC complexes was successful. Furthermore, primary, secondary and tertiary structure of Nsp6 and Nsp6-MSP1E3D1-POPC complexes were characterized using different biophysical measurements. Primary structure analysis could show the molecular

weight of Nsp6 being 34.29 kDa, indicating the purified protein to be complete. The secondary structure analysis was able to confirm alpha helical model by AlphaFold using circular dichroism spectroscopy analysis. Tertiary structure analysis revealed buried tryptophan and a high average distance between tryptophan and tyrosine due to low energy transfer measured via fluorescence spectroscopy. Moreover, oligomerization state analysis using mass photometry revealed that Nsp6 incorporates as a dimer into the nanodiscs. But in general, Nsp6-nanodisc complexes seem to be highly unstable during experiments, leading to the assumption that POPC may not be considered best for incorporating Nsp6. Since Nsp6 is mainly found in DMVs formed by the ER, the lipid composition of these membrane structures should be figured out in order to prepare nanodiscs with proper lipid composition.

However, further biophysical measurements need to be done like microscale thermophoresis assay, bio-layer interferometry analysis or isothermal titration calorimetry analysis to prove Nsp6 to be functional by binding it to different inhibitors like haloperidol hydrochloride and dextromethorphan hydrobromide. To facilitate alignment of particles, Nsp6 needs to be recloned with additional mass of known protein like GFP to analyze its structure using cryogenic electron microscopy. Additionally, addition of isotope labelled amino acids into *in vitro* reaction could allow performing NMR (nuclear magnetic resonance) spectroscopy analysis of Nsp6-MSP1E3D1-POPC complexes to pursuit the structure solution.

Literature

- [1] J. D. Cherry, "The chronology of the 2002–2003 SARS mini pandemic," *Paediatr. Respir. Rev.*, vol. 5, no. 4, p. 262, Dec. 2004, doi: 10.1016/J.PRRV.2004.07.009.
- [2] M. Chan-Yeung and R. H. Xu, "SARS: epidemiology," *Respirology*, vol. 8, no. Suppl 1, p. S9, Nov. 2003, doi: 10.1046/J.1440-1843.2003.00518.X.
- [3] A. M. Zaki, S. van Boheemen, T. M. Bestebroer, A. D. M. E. Osterhaus, and R. A. M. Fouchier, "Isolation of a Novel Coronavirus from a Man with Pneumonia in Saudi Arabia," *N. Engl. J. Med.*, vol. 367, no. 19, pp. 1814–1820, Nov. 2012, doi: 10.1056/NEJMOA1211721/SUPPL_FILE/NEJMOA1211721_DISCLOSURES.PDF.
- [4] A. R. Zhang, W. Q. Shi, K. Liu, X. Lou Li, M. J. Liu, W. H. Zhang, G. P. Zhao, J. J. Chen, X. A. Zhang, D. Miao, W. Ma, W. Liu, Y. Yang, and L. Q. Fang, "Epidemiology and evolution of Middle East respiratory syndrome coronavirus, 2012–2020," *Infect. Dis. Poverty*, vol. 10, no. 1, pp. 1–13, Dec. 2021, doi: 10.1186/S40249-021-00853-0/FIGURES/3.
- [5] M. Ciotti, S. Angeletti, M. Minieri, M. Giovannetti, D. Benvenuto, S. Pascarella, C. Sagnelli, M. Bianchi, S. Bernardini, and M. Ciccozzi, "COVID-19 Outbreak: An Overview," *Chemotherapy*, vol. 64, no. 5–6, pp. 215–223, Jul. 2019, doi: 10.1159/000507423.
- [6] "WHO erklärt COVID-19-Ausbruch zur Pandemie," Mar. 2020.
- [7] "ICTV." <https://talk.ictvonline.org/taxonomy/> (accessed Dec. 09, 2021).
- [8] C. Huang, Y. Wang, X. Li, L. Ren, J. Zhao, Y. Hu, L. Zhang, G. Fan, J. Xu, X. Gu, *et al.*, "Clinical features of patients infected with 2019 novel coronavirus in Wuhan, China," *Lancet (London, England)*, vol. 395, no. 10223, pp. 497–506, Feb. 2020, doi: 10.1016/S0140-6736(20)30183-5.
- [9] Q. Li, X. Guan, P. Wu, X. Wang, L. Zhou, Y. Tong, R. Ren, K. S. M. Leung, E. H. Y. Lau, J. Y. Wong, *et al.*, "Early Transmission Dynamics in Wuhan, China, of Novel Coronavirus–Infected Pneumonia," *N. Engl. J. Med.*, vol. 382, no. 13, pp. 1199–1207, Mar. 2020, doi: 10.1056/NEJMOA2001316.
- [10] C. Huang, Y. Wang, X. Li, L. Ren, J. Zhao, Y. Hu, L. Zhang, G. Fan, J. Xu, X. Gu, *et al.*, "Clinical features of patients infected with 2019 novel coronavirus in Wuhan, China," *Lancet*, vol. 395, no. 10223, pp. 497–506, Feb. 2020, doi: 10.1016/S0140-6736(20)30183-5.
- [11] N. Ram-Mohan, D. Kim, E. J. Zudock, M. M. Hashemi, K. C. Tjandra, A. J. Rogers, C. A. Blish, K. C. Nadeau, J. A. Newberry, J. V. Quinn, *et al.*, "SARS-CoV-2 RNAemia Predicts Clinical Deterioration and Extrapulmonary Complications from COVID-19," *Clin. Infect. Dis.*, vol. 74, no. 2, pp. 218–226, Jan. 2022, doi: 10.1093/CID/CIAB394.

- [12] L. Li, Q. Huang, D. C. Wang, D. H. Ingbar, and X. Wang, "Acute lung injury in patients with COVID-19 infection," *Clin. Transl. Med.*, vol. 10, no. 1, pp. 20–27, Mar. 2020, doi: 10.1002/CTM2.16.
- [13] W. Wang, J. Tang, and F. Wei, "Updated understanding of the outbreak of 2019 novel coronavirus (2019-nCoV) in Wuhan, China," *J. Med. Virol.*, vol. 92, no. 4, pp. 441–447, Apr. 2020, doi: 10.1002/JMV.25689.
- [14] E. Mahase, "Covid-19: What do we know about 'long covid'?", *BMJ*, vol. 370, Jul. 2020, doi: 10.1136/BMJ.M2815.
- [15] A. Synowiec, A. Szczepański, E. Barreto-Duran, L. K. Lie, and K. Pyrc, "Severe acute respiratory syndrome coronavirus 2 (SARS-CoV-2): A systemic infection," *Clin. Microbiol. Rev.*, vol. 34, no. 2, pp. 1–32, Apr. 2021, doi: 10.1128/CMR.00133-20/ASSET/9B472912-235C-4EAF-925C-6D9628B48DA1/ASSETS/GRAPHIC/CMR.00133-20-F0006.JPEG.
- [16] Z. Ke, J. Oton, K. Qu, M. Cortese, V. Zila, L. McKeane, T. Nakane, J. Zivanov, C. J. Neufeldt, B. Cerikan, *et al.*, "Structures and distributions of SARS-CoV-2 spike proteins on intact virions," *Nat. 2020 5887838*, vol. 588, no. 7838, pp. 498–502, Aug. 2020, doi: 10.1038/s41586-020-2665-2.
- [17] Y. Watanabe, J. D. Allen, D. Wrapp, J. S. McLellan, and M. Crispin, "Site-specific glycan analysis of the SARS-CoV-2 spike," *Science*, vol. 369, no. 6501, pp. 330–333, Jul. 2020, doi: 10.1126/SCIENCE.ABB9983.
- [18] B. Turoňová, M. Sikora, C. Schürmann, W. J. H. Hagen, S. Welsch, F. E. C. Blanc, S. von Bülow, M. Gecht, K. Bagola, C. Hörner, *et al.*, "In situ structural analysis of SARS-CoV-2 spike reveals flexibility mediated by three hinges," *Science*, vol. 370, no. 6513, p. 203, Oct. 2020, doi: 10.1126/SCIENCE.ABD5223.
- [19] H. Yao, Y. Song, Y. Chen, N. Wu, J. Xu, C. Sun, J. Zhang, T. Weng, Z. Zhang, Z. Wu, *et al.*, "Molecular Architecture of the SARS-CoV-2 Virus," *Cell*, vol. 183, no. 3, pp. 730–738.e13, Oct. 2020, doi: 10.1016/J.CELL.2020.09.018.
- [20] V. S. Mandala, M. J. McKay, A. A. Shcherbakov, A. J. Dregni, A. Kolocouris, and M. Hong, "Structure and drug binding of the SARS-CoV-2 envelope protein transmembrane domain in lipid bilayers," *Nat. Struct. Mol. Biol. 2020 2712*, vol. 27, no. 12, pp. 1202–1208, Nov. 2020, doi: 10.1038/s41594-020-00536-8.
- [21] S. Kumar, R. Nyodu, V. K. Maurya, and S. K. Saxena, "Morphology, Genome Organization, Replication, and Pathogenesis of Severe Acute Respiratory Syndrome Coronavirus 2 (SARS-CoV-2)," *Coronavirus Dis. 2019*, p. 23, 2020, doi: 10.1007/978-981-15-4814-7_3.
- [22] J. Cui, F. Li, and Z. L. Shi, "Origin and evolution of pathogenic coronaviruses," *Nat. Rev. Microbiol.*, vol. 17, no. 3, pp. 181–192, Mar. 2019, doi: 10.1038/S41579-018-

- 0118-9.
- [23] C.-S. Shi, H.-Y. Qi, C. Boullaran, N.-N. Huang, M. Abu-Asab, J. H. Shelhamer, and J. H. Kehrl, "SARS-coronavirus open reading frame-9b suppresses innate immunity by targeting mitochondria and the MAVS/TRAF3/TRAF6 signalosome," *J. Immunol.*, vol. 193, no. 6, pp. 3080–3089, Sep. 2014, doi: 10.4049/JIMMUNOL.1303196.
- [24] A. A. T. Naqvi, K. Fatima, T. Mohammad, U. Fatima, I. K. Singh, A. Singh, S. M. Atif, G. Hariprasad, G. M. Hasan, and M. I. Hassan, "Insights into SARS-CoV-2 genome, structure, evolution, pathogenesis and therapies: Structural genomics approach," *Biochim. Biophys. Acta. Mol. Basis Dis.*, vol. 1866, no. 10, Oct. 2020, doi: 10.1016/J.BBADIS.2020.165878.
- [25] S. Su, G. Wong, W. Shi, J. Liu, A. C. K. Lai, J. Zhou, W. Liu, Y. Bi, and G. F. Gao, "Epidemiology, Genetic Recombination, and Pathogenesis of Coronaviruses," *Trends Microbiol.*, vol. 24, no. 6, p. 490, Jun. 2016, doi: 10.1016/J.TIM.2016.03.003.
- [26] B. BJ, van der Z. R, de H. CA, and R. PJ, "The coronavirus spike protein is a class I virus fusion protein: structural and functional characterization of the fusion core complex," *J. Virol.*, vol. 77, no. 16, pp. 8801–8811, Aug. 2003, doi: 10.1128/JVI.77.16.8801-8811.2003.
- [27] L. Guruprasad, "Human SARS CoV-2 spike protein mutations," 2021, doi: 10.1002/prot.26042.
- [28] S. Belouzard, J. K. Millet, B. N. Licitra, and G. R. Whittaker, "Mechanisms of coronavirus cell entry mediated by the viral spike protein," *Viruses*, vol. 4, no. 6, pp. 1011–1033, 2012, doi: 10.3390/V4061011.
- [29] J. Pollet, W.-H. Chen, and U. Strych, "Recombinant protein vaccines, a proven approach against coronavirus pandemics," 2021, doi: 10.1016/j.addr.2021.01.001.
- [30] X. S, Z. Y, L. M, L. Q, X. W, W. Y, Y. T, L. S, S. Z, J. S, and L. L, "Fusion mechanism of 2019-nCoV and fusion inhibitors targeting HR1 domain in spike protein," *Cell. Mol. Immunol.*, vol. 17, no. 7, pp. 765–767, Jul. 2020, doi: 10.1038/S41423-020-0374-2.
- [31] S. Belouzard, V. C. Chu, and G. R. Whittaker, "Activation of the SARS coronavirus spike protein via sequential proteolytic cleavage at two distinct sites," *Proc. Natl. Acad. Sci. U. S. A.*, vol. 106, no. 14, p. 5871, Apr. 2009, doi: 10.1073/PNAS.0809524106.
- [32] N. Iwata-Yoshikawa, T. Okamura, Y. Shimizu, H. Hasegawa, M. Takeda, and N. Nagata, "TMPRSS2 Contributes to Virus Spread and Immunopathology in the Airways of Murine Models after Coronavirus Infection," *J. Virol.*, vol. 93, no. 6, pp. 1815–1833, Mar. 2019, doi: 10.1128/JVI.01815-18.
- [33] M. Hoffmann, H. Kleine-Weber, S. Schroeder, N. Krüger, T. Herrler, S. Erichsen, T. S. Schiergens, G. Herrler, N. H. Wu, A. Nitsche, M. A. Müller, C. Drosten, and S. Pöhlmann, "SARS-CoV-2 Cell Entry Depends on ACE2 and TMPRSS2 and Is Blocked

- by a Clinically Proven Protease Inhibitor,” *Cell*, vol. 181, no. 2, p. 271, Apr. 2020, doi: 10.1016/J.CELL.2020.02.052.
- [34] H. Kleine-Weber, M. T. Elzayat, M. Hoffmann, and S. Pöhlmann, “Functional analysis of potential cleavage sites in the MERS-coronavirus spike protein,” *Sci. Rep.*, vol. 8, no. 1, Dec. 2018, doi: 10.1038/S41598-018-34859-W.
- [35] J. K. Millet and G. R. Whittaker, “Physiological and molecular triggers for SARS-CoV membrane fusion and entry into host cells,” *Virology*, vol. 517, p. 3, Apr. 2018, doi: 10.1016/J.VIROL.2017.12.015.
- [36] Y. Zhu, F. Feng, G. Hu, Y. Wang, Y. Yu, Y. Zhu, W. Xu, X. Cai, Z. Sun, W. Han, *et al.*, “A genome-wide CRISPR screen identifies host factors that regulate SARS-CoV-2 entry,” *Nat. Commun.*, vol. 12, no. 1, Dec. 2021, doi: 10.1038/S41467-021-21213-4.
- [37] B. Malone, N. Urakova, E. J. Snijder, and E. A. Campbell, “Structures and functions of coronavirus replication–transcription complexes and their relevance for SARS-CoV-2 drug design,” *Nat. Rev. Mol. Cell Biol.* 2021 231, vol. 23, no. 1, pp. 21–39, Nov. 2021, doi: 10.1038/s41580-021-00432-z.
- [38] P. V’kovski, A. Kratzel, S. Steiner, H. Stalder, and V. Thiel, “Coronavirus biology and replication: implications for SARS-CoV-2,” *Nat. Rev. Microbiol.* 2020 193, vol. 19, no. 3, pp. 155–170, Oct. 2020, doi: 10.1038/s41579-020-00468-6.
- [39] G. Wolff, C. E. Melia, E. J. Snijder, and M. Bárcena, “Double-Membrane Vesicles as Platforms for Viral Replication,” *Trends Microbiol.*, vol. 28, no. 12, pp. 1022–1033, Dec. 2020, doi: 10.1016/J.TIM.2020.05.009.
- [40] E. M. Scutigliani and M. Kikkert, “Interaction of the innate immune system with positive-strand RNA virus replication organelles,” *Cytokine Growth Factor Rev.*, vol. 37, pp. 17–27, Oct. 2017, doi: 10.1016/J.CYTOGFR.2017.05.007.
- [41] J. Pan, X. Peng, Y. Gao, Z. Li, X. Lu, Y. Chen, M. Ishaq, D. Liu, M. L. DeDiego, L. Enjuanes, and D. Guo, “Genome-Wide Analysis of Protein-Protein Interactions and Involvement of Viral Proteins in SARS-CoV Replication,” *PLoS One*, vol. 3, no. 10, p. e3299, Oct. 2008, doi: 10.1371/JOURNAL.PONE.0003299.
- [42] M. M. Angelini, M. Akhlaghpour, B. W. Neuman, and M. J. Buchmeier, “Severe Acute Respiratory Syndrome Coronavirus Nonstructural Proteins 3, 4, and 6 Induce Double-Membrane Vesicles,” *MBio*, vol. 4, no. 4, Aug. 2013, doi: 10.1128/MBIO.00524-13.
- [43] D. Oudshoorn, K. Rijs, R. W. A. L. Limpens, K. Groen, A. J. Koster, E. J. Snijder, M. Kikkert, and M. Bárcena, “Expression and Cleavage of Middle East Respiratory Syndrome Coronavirus nsp3-4 Polyprotein Induce the Formation of Double-Membrane Vesicles That Mimic Those Associated with Coronaviral RNA Replication,” *MBio*, vol. 8, no. 6, pp. 1658–1675, Nov. 2017, doi: 10.1128/MBIO.01658-17.
- [44] E. M. Cottam, H. J. Maier, M. Manifava, L. C. Vaux, P. Chandra-Schoenfelder, W.

- Gerner, P. Britton, N. T. Ktistakis, and T. Wileman, "Coronavirus nsp6 proteins generate autophagosomes from the endoplasmic reticulum via an omegasome intermediate," *Autophagy*, vol. 7, no. 11, pp. 1335–1347, 2011, doi: 10.4161/AUTO.7.11.16642.
- [45] X. Sun, Y. Liu, Z. Huang, W. Xu, W. Hu, L. Yi, Z. Liu, H. Chan, J. Zeng, X. Liu, *et al.*, "SARS-CoV-2 non-structural protein 6 triggers NLRP3-dependent pyroptosis by targeting ATP6AP1," *Cell Death Differ. 2021*, pp. 1–15, Jan. 2022, doi: 10.1038/s41418-021-00916-7.
- [46] S. Ricciardi, A. M. Guarino, L. Giaquinto, E. V. Polishchuk, M. Santoro, G. Di Tullio, C. Wilson, F. Panariello, V. C. Soares, S. S. G. Dias, *et al.*, "The role of NSP6 in the biogenesis of the SARS-CoV-2 replication organelle," *Nature*, vol. 606, no. 7915, pp. 761–768, Jun. 2022, doi: 10.1038/S41586-022-04835-6.
- [47] S. Raran-Kurussi, S. Cherry, D. Zhang, and D. S. Waugh, "Removal of Affinity Tags with TEV Protease," *Methods Mol. Biol.*, vol. 1586, p. 221, 2017, doi: 10.1007/978-1-4939-6887-9_14.
- [48] S. Ricciardi, A. M. Guarino, L. Giaquinto, E. V. Polishchuk, M. Santoro, G. Di Tullio, C. Wilson, F. Panariello, V. C. Soares, S. S. G. Dias, *et al.*, "The role of NSP6 in the biogenesis of the SARS-CoV-2 replication organelle," *Nat. 2022 6067915*, vol. 606, no. 7915, pp. 761–768, May 2022, doi: 10.1038/s41586-022-04835-6.
- [49] J. Spainhour, M. G. Janech, J. H. Schwacke, J. Velez, and V. Ramakrishnan, "The Application of Gaussian Mixture Models for Signal Quantification in MALDI-ToF Mass Spectrometry of Peptides," *PLoS One*, vol. 9, no. 11, p. 111016, 2014, doi: 10.1371/journal.pone.0111016.
- [50] "Tips and tricks for successful Mass spec experiments | Proteintech Group." <https://www.ptglab.com/news/blog/tips-and-tricks-for-successful-mass-spec-experiments/> (accessed Sep. 24, 2022).
- [51] S. Niebling, K. Veith, B. Vollmer, J. Lizarrondo, O. Burastero, J. Schiller, A. Struve García, P. Lewe, C. Seuring, S. Witt, and M. García-Alai, "Biophysical Screening Pipeline for Cryo-EM Grid Preparation of Membrane Proteins," *Front. Mol. Biosci.*, vol. 9, p. 535, Jun. 2022, doi: 10.3389/FMOLB.2022.882288/BIBTEX.
- [52] D. Ringe and G. A. Petsko, "The 'glass transition' in protein dynamics: what it is, why it occurs, and how to exploit it," *Biophys. Chem.*, vol. 105, no. 2–3, pp. 667–680, Sep. 2003, doi: 10.1016/S0301-4622(03)00096-6.
- [53] Y. K. Reshetnyak and E. A. Burstein, "Decomposition of Protein Tryptophan Fluorescence Spectra into Log-Normal Components. II. The Statistical Proof of Discreteness of Tryptophan Classes in Proteins," *Biophys. J.*, vol. 81, no. 3, pp. 1710–1734, Sep. 2001, doi: 10.1016/S0006-3495(01)75824-9.

- [54] C. Duy and J. Fitter, "How Aggregation and Conformational Scrambling of Unfolded States Govern Fluorescence Emission Spectra," *Biophys. J.*, vol. 90, no. 10, pp. 3704–3711, May 2006, doi: 10.1529/BIOPHYSJ.105.078980.
- [55] K. E. Sapsford, L. Berti, and I. L. Medintz, "Materials for Fluorescence Resonance Energy Transfer Analysis: Beyond Traditional Donor-Acceptor Combinations**," doi: 10.1002/anie.200503873.

Eidesstattliche Erklärung

Ich versichere, dass ich die vorliegende Arbeit ohne fremde Hilfe selbständig verfasst und nur die angegebenen Quellen und Hilfsmittel benutzt habe. Wörtlich oder dem Sinn nach aus anderen Werken entnommene Stellen sind unter Angabe der Quelle kenntlich gemacht.

Erklärung –Einverständnis

Ich erkläre mich damit

einverstanden,

nicht einverstanden

dass ein Exemplar meiner Master Thesis in die Bibliothek des Fachbereichs aufgenommen wird; Rechte Dritter werden dadurch nicht verletzt

Ort, Datum

Unterschrift